Differentiating eelgrass (*Z. marina*), finger kelp (*L. digitata*), and sugar kelp (*S. latissima*) at the Eastern Shore Islands, Nova Scotia, using PRISMA hyperspectral satellite imagery

Neve Sophie Foreman

Thesis submitted to the University of Ottawa
in partial fulfillment of the requirements for the
Master of Science in Geography

Department of Geography, Environment and Geomatics
Faculty of Arts
University of Ottawa

Thesis Supervisor: Anders Knudby

© Neve Sophie Foreman, Ottawa, Canada, 2026

Abstract

Laminaria digitata (finger kelp), *Saccharina latissima* (sugar kelp), and *Zostera marina* (eelgrass) are three marine macrophytes whose habitats are known as blue carbon ecosystems due to their outstanding carbon sequestration capabilities. All three species are found at the Eastern Shore Islands (ESI), Nova Scotia, an Area of Interest (AOI) for ecological and biological importance. It is important to distinguish these species, as they have different suitable water temperature ranges, contribute to the blue carbon ecosystem in different ways, and are at threat due to climate change. Previous regional studies using multispectral satellite sensors to map marine macrophytes were unsuccessful at differentiating eelgrass from brown algae, but a hyperspectral satellite sensor offers the high spectral resolution (many bands <15nm wide) that is needed for detecting subtle differences between species. This thesis assessed the ability of PRISMA 30m spatial resolution hyperspectral satellite imagery to map eelgrass, finger kelp, and sugar kelp using an area near Sheet Harbour, Nova Scotia, within the ESI AOI, as a study site. In July 2025, in-situ data was collected by drop camera survey to confirm absence or presence of target species, then combined with the spectral information from a PRISMA image taken on August 7, 2025. Six different RF models were trained and tested on the PRISMA data. We also trained and tested two models using a Landsat-9 multispectral satellite image from July 27, 2025. A >10% increase in accuracy was achieved by using the PRISMA hyperspectral satellite image over the Landsat-9 image (up to 49.2% balanced accuracy compared to 36.0%). The two highest performing PRISMA models both included depth information, either directly or through a correction to obtain bottom reflectance. This study represents an improvement in differentiating brown algae from eelgrass in the region, as eelgrass habitat was predicted at up to 57% recall, and finger kelp habitat was predicted at up to 71% recall. Further studies should focus on better mapping sugar kelp (recall <5%), as the heterogeneity of species in this region likely affects the models' accuracy.

Acknowledgements

Thank you to all my friends and family who have supported me during the completion of this thesis. I would like to extend a very big thank you to Zachary Guindon for his assistance and iii involvement in the drop camera survey sampling. Not only did Zach assist in drafting the design and assembly of the drop camera frame, but he gave up two weeks of his time to act as field assistant for the drop camera survey. Without his help, the in-situ data collection would not have been possible. I would also like to extend a big thank you to my supervisor, Anders Knudby, for his support and guidance throughout this process, and to my committee, Charles Brunette and Emmanuel Devred for their support and helpful suggestions. Thank you to the locals of Nova Scotia for their hospitality, including Scott Cunningham at Coastal Adventures and the owner of 443 Mozier Cove Rd. Finally, thank you to those who assisted with the fieldwork by loaning or helping to build equipment, including the Department of Geography, Sherri, SWEOL, and the staff of uOttawa Makerspace.

Table of Contents

ABSTRACT ..... **II**

ACKNOWLEDGEMENTS ..... **III**

LIST OF FIGURES ..... **IV**

LIST OF TABLES ..... **VI**

LIST OF ACRONYMS ..... **VI**

CHAPTER 1: INTRODUCTION **1**

1.1 CONTEXT 1

1.1.1 The threat of climate change and other factors on eelgrass and kelps in Nova Scotia **1**

1.1.2 Finger kelp, sugar kelp, and eelgrass as sources of carbon sequestration and their other important benefits **3**

1.1.3 Principles behind the remote sensing of marine macrophytes **4**

1.2 OBJECTIVES 5

1.3 THESIS FORMAT 5

1.4 DROP CAMERA SURVEY APPROACH 5

CHAPTER 2: DIFFERENTIATING EELGRASS (*Z. MARINA*), FINGER KELP (*L. DIGITATA*), AND SUGAR KELP (*S. LATISSIMA*) AT THE EASTERN SHORE ISLANDS, NOVA SCOTIA, USING PRISMA HYPERSPECTRAL SATELLITE IMAGERY 6

ABSTRACT 6
2.1 INTRODUCTION 7
2.2 STUDY AREA 10
2.3 METHODOLOGY 11
2.3.1 Hyperspectral satellite tasking and image processing 12
2.3.2 Multispectral image acquisition and processing 14
2.3.3 In-situ data collection 15
2.3.4 In-situ data annotation 18
2.3.5 Machine learning features from PRISMA imagery 21
2.3.6 Dataset size, sorting, and machine learning process 21
2.3.7 Random forest model definitions 23
2.3.8 Machine learning feature reduction 25
2.3.9 Machine learning model training and evaluation 25
2.3.10 Final model training 26
2.4 RESULTS 26
2.4.1 Drop camera survey 26
2.4.2 Feature elimination 29
2.4.3 Machine learning model results 32
2.4.4 Landsat-9 model performance 37
2.5 DISCUSSION 39
2.5.1 In-situ data collection and species distribution 39
2.5.2 Model results and hyperspectral satellite imagery 40
2.5.3 Recommendations for future work 41
2.6 CONCLUSION 42
2.7 AUTHOR CONTRIBUTIONS 42
2.8 REFERENCES 42
2.9 APPENDIX 52

CHAPTER 3: THESIS CONCLUSION 56

AI USE DECLARATION 58

List of Figures

Figure 1. A: Small-scale map showing the approximate boundary of the ESI AOI in relation to Halifax, Nova Scotia, and the study site at Sheet Harbour. B: Large-scale map showing the study site, off the coast of Sheet Harbour. 11
Figure 2. Flowchart outlining the process of in-situ and satellite data collection, processing, and training and testing. Each number corresponds to a section below that provides more details. . 12

Figure 3. The 446nm from the PRISMA image acquired August 7th, 2025, shows overall good quality with some striping noise. 13
Figure 4. Landsat-9 image, single band (blue: 450-510nm), no visible striping noise. 15
Figure 5. Drop camera survey sampling point scheme near Sheet Harbour, NS. Each point corresponds to a location where a 3-minute video was taken. 17
Figure 6. A: Drop camera frame design prior to attaching rope. B: Drop camera frame during deployment. 17
Figure 7. Examples of the three target species: eelgrass, finger kelp, and sugar kelp. 19
Figure 8. Example of photo for annotation. This photo, M6-1, was annotated with 25% sugar kelp, 0% eelgrass, 5% finger kelp, and 75% other vegetation. 20
Figure 9. Data sorting and machine learning process flowchart. Further details on Random Forest Recursive Feature Elimination (RF-RFE) and model training can be found in sections 2.3.8 and 2.3.9. Each fold has an approximate, not exact, 70% to 30% split. 22
Figure 10. Heterogeneity (co-occurrence) of sugar kelp and finger kelp (>5% percent cover of each species). 27
Figure 11. Still shot from the drop camera survey demonstrating heterogeneity between species. A: sugar kelp, B: finger kelp, and C: 'other vegetation.' 28
Figure 12. Average line of the spectral signatures of each class, in addition to optically deep water, derived from all admissible data (less than or equal to 10m depth) and the PRISMA single band values across the visible spectrum. 29
Figure 13. Shows the distribution of the most frequently selected PRISMA features (retained in 60% or more folds, excluding K and KD) across the spectrum of light and in relation to the relevant Landsat-9 OLI-2 bands. 31
Figure 14. Feature elimination plot from full model M including balanced accuracy and MCC. Feature elimination proceeds iteratively from right to left in these plots. 31
Figure 15. Confusion matrices of models RD and M as averages of all 5-folds during the testing stage. Row-normalized as the values were averaged across all 5-folds of the training and testing stage. 34
Figure 16. Output classification map from the highest performing model, RD. A: locations of identified eelgrass patches; B: locations of identified finger kelp habitat. 35
Figure 17. Output predicted probability map for finger kelp (model M), which had recall of >70% during the testing stage. 36
Figure 18. Model M prediction at points K6-1 to K6-7 with reference to original in-situ data. ... 37
Figure 19. Confusion matrix for the Landsat-9 model, L9. Row-normalized as the values were averaged across all 5-folds of the training and testing stage. 38
Figure 20. Output classification map from highest performing Landsat-9 model, LD. 39
Figure 21. Example of rocky/sandy unvegetated substrate. Point D11-5. 52
Figure 22. Example of finger and sugar kelp growing heterogeneously. Point J6-5 53
Figure 23. Example of the types of vegetation found at the intertidal zones very close to shore including Fucus distichus (rockweed) and Fucus spiralis (spiral wrack). Point I6-5. 53
Figure 24. Example of Saccorhiza dermatodea, another brown alga. Point K3-2 54
Figure 25. Example of Desmarestia (shown centre). Point M6-6. 54

Figure 26. Example of Agarum clathratum, another brown alga, shown at right (and upper middle), and other marine macrophyte species, center. Point I3-1. ..... *55*
Figure 27. Invasive Codium Fragile, shown middle. Point K6-4. ..... *55*
Figure 28. Drop camera frame setup attached to kayak. *56*

List of Tables

Table 1. Size (# of raster cells) of each class for the standard vegetation class rule (10m depth threshold). *22*
Table 2. Description of all models used and their features. *23*
Table 3. Top features selected - in 60% or more of PRISMA models' folds (excluding models K and KD) *29*
Table 4. Model results summary. *32*

List of Acronyms

AOI	Area of Interest
CD	Chart Datum
CHS NONNA	Canadian Hydrographic Service Non-Navigational
ESI	Eastern Shore Islands
MCC	Matthews Correlation Coefficient
NPP	Net Primary Production
ODW	Optically Deep Water
OSW	Optically Shallow Water
PRISMA	PRecursore IperSpettrale della Missione Applicative / Hyperspectral Precursor of the Application Mission
SSB	Scotian Shelf Bioregion
SST	Sea Surface Temperature
SWIR	Short-Wave InfraRed
VNIR	Visible and Near-InfraRed

Chapter 1: Introduction

1.1 Context

Laminaria digitata (finger kelp), *Saccharina latissima* (sugar kelp), and *Zostera marina* (eelgrass) are three marine macrophytes whose habitats include the Eastern Shore Islands (ESI), Nova Scotia. The habitats of many marine macrophytes, including eelgrass and kelps, are known as blue carbon ecosystems due to their outstanding carbon sequestration capabilities. These species are biologically distinct, have different suitable habitats and add value to the blue carbon ecosystem for different reasons (Bartsch et al., 2008). Seagrass environments account for up to 33% of total oceanic CO_2 uptake, while kelps forests in Nova Scotia are estimated to sequester more carbon than eelgrass by ~1.3 orders of magnitude largely due to the role of export of dissolved organic carbon and their large habitat size (Alongi, 2018; Krumhansl et al., 2026; Röhr et al., 2018; Wright et al., 2022). Due largely to ocean warming and marine heat waves, finger and sugar kelp have had significant habitat loss (Filbee-Dexter & Wernberg, 2018); eelgrass has experienced habitat loss in some areas but is projected to have habitat gain in other areas (Wilson & Lotze, 2019). As eelgrass, sugar kelp, and finger kelp are all foundational species, the loss of populations causes negative changes at the ecosystem level (King et al., 2025; Wernberg et al., 2019).

The research in this thesis was conducted off the coast of Sheet Harbour, Nova Scotia, Canada, within the Eastern Shore Islands (ESI) Area of Interest (AOI). The ESI were identified as an AOI by the Department of Fisheries and Oceans (DFO) in February 2018. A marine AOI is defined as such when a criterion is met for biological and ecological importance in a unique geographical location (Department of Fisheries and Oceans Canada, 2024). The site was selected due to having known high populations of *L. digitata*, *S. latissima*, and *Z. marina*, which are the example species in this case study (Krumhansl et al., 2024). The study area is small, approximately 40km^2, with ~13 km^2 covered by shallow coastal water <10m deep, to ensure that in-depth field surveys could be carried out by sea kayak, while covering many potential patches of benthic habitat.

1.1.1 The threat of climate change and other factors on eelgrass and kelps in Nova Scotia

The Eastern Shore Islands are part of the Scotian Shelf Bioregion (SSB), which has cold temperate waters and experiences seasonal cold-water circulation (Brickman et al., 2016; Han et

al., 1999). The SSB is showing a 0.37-0.39^{0}C ± 0.06^{0}C per decade trend in rising 2 sea surface temperature (SST), which is an average and does not individually consider seasonal differences or heat waves (Chen et al., 2020; Thomas et al., 2017). Marine heat waves can be detrimental as they result in high rates of kelp mortality, reduced growth, and increased mortality in eelgrass (Filbee-Dexter et al., 2020; Hammer et al., 2018). There are other factors associated with climate change that will affect marine macrophytes, such as changing storm patterns, as more frequent storms could lead to a significant decline in kelp forest diversity and eelgrass population directly (Byrnes et al., 2011; Krumhansl et al., 2020). While overall warming is occurring at the SSB, the ESI, including our study area at Sheet Harbour, has colder mean annual temperatures in comparison to other areas within the SSB (Brickman et al., 2016; Han et al., 1999; Jabbari et al., 2024).

Finger and sugar kelp can only survive in waters up to 22-23^{0}C; moreover, finger kelp grows more slowly and experiences peak growth at 10^{0}C, while sugar kelp shows optimal growth at 10-15^{0}C (Bolton & Lüning, 1982). Kelp sporophytes are also sensitive to heat (Bartsch et al., 2013). Therefore, increasing average SST reduces optimal growth and reproduction, while heatwaves significantly increase mortality in both kelps (Bartsch et al., 2013; Drew, 1983). Though eelgrass is adapted to warmer temperatures than finger kelp, it also experiences decreased growth and mortality at higher temperatures (Jabbari et al., 2024). Eelgrass is already decreasing at -1.4% per year worldwide based on 126 studies, ~4% of seagrass was lost between 2019 to 2024, and eelgrass in the Northwest Atlantic is projected to shift northward by as much as 6.48ºN by 2100 under a 'business as usual' climate change scenario (Peng et al., 2026; Short et al., 2011; Wilson & Lotze, 2019). The maximum survivable temperature for eelgrass seedlings is ~28ºC, and at 30ºC, mature shoots experience increased mortality; however, the optimal range for young seedling growth is only 16-17^{0}C (Hammer et al., 2018; Niu et al., 2012). While this is much higher than the survivable temperature of both kelps, eelgrass is still at risk. Moreover, eelgrass has an additional threat it is facing that finger kelp does not: eelgrass in Atlantic Canada is at risk from the invasive green crab through damage to roots and rhizomes and disrupting sediment during the process of digging to feed on invertebrates and other prey, or burrowing for shelter (Malyshev & Quijón, 2011; Matheson et al., 2016). Many green crabs were identified in sandy areas at the study site, further emphasizing the risk to eelgrass habitat.

1.1.2 Finger kelp, sugar kelp, and eelgrass as sources of carbon sequestration and their other important benefits

Finger kelp, sugar kelp and eelgrass all play important roles in the marine environment – both as direct and indirect sources of carbon sequestration, and as important engineers in the underwater landscape. Eelgrass's contribution to carbon accumulation per unit area is up to 3 orders of magnitude higher than terrestrial soils, and seagrass environments account for up to 33% of total oceanic CO_2 uptake (Röhr et al., 2018). Not only does the direct storage of carbon in eelgrass contribute to this overall effect, but so does the storage in sediment via burial and subsequent export to elsewhere in the ocean (Duarte & Krause-Jensen, 2017). Finger and sugar kelp also have an important contribution towards carbon sequestration, with the highest percentage of their total net primary production (NPP) being export at 43.5%, compared to only 24.3% for seagrass (Duarte, 2017). The carbon sequestration in seagrass beds is a more direct effect, mainly in sediment burial and some via export, while macroalgae sequesters carbon mainly by transport to deep sea, through macroalgal material drifting through submarine canyons, and the sinking of negatively buoyant macroalgal detritus (Krause-Jensen & Duarte, 2016). In Nova Scotia, the contribution of export for both eelgrass and kelps is estimated to be even higher than estimated globally (Krumhansl et al., 2026). Mapping marine macrophyte habitats by species is important for understanding both the overall carbon sequestration contribution of marine macrophytes, and the specific allocation of each mechanism towards their NPP.

In addition to both eelgrass and kelps' carbon sequestration capabilities, they all have an important role in the marine environments, mainly by providing habitat for juvenile fish and other species such as snails. Eelgrass beds not only provide habitat for numerous species but have been shown as a habitat that is used preferentially for many species, and there is no other substitute species that will grow on sand or mud flats (Department of Fisheries and Oceans Canada, 2009). The species that rely on eelgrass include, but are not limited to, fish, invertebrates, and birds. Eelgrass beds have high levels of primary production and are critical for creating structure, food, and providing shelter within the intertidal and subtidal zones (Murphy et al., 2021). Brown algae, including sugar and finger kelp, also provide structure and shelter for many organisms, including juvenile fish, similarly to eelgrass, and grow on rocky substrates, primarily within the 2.5 to 10m depth range, but can grow as deep as 30 meters (Adey & Hayek, 2011; James & Whitfield, 2023; Mathieson & Dawes, 2020).

1.1.3 Principles behind the remote sensing of marine macrophytes

Marine macrophytes can be detected and differentiated in optically shallow water (OSW) using optical remote sensing techniques due to their ability to reflect and absorb light. In OSW, light may be reflected from the bottom in an amount detectable by a satellite sensor; therefore, the bottom habitat will affect the overall reading of light captured by the sensor. In the visible spectrum, submerged vegetation can be detected similarly to the way vegetation is detected on land: the composition of different pigments, especially chlorophylls, dictates how plants absorb and reflect light; as such, each plant has a unique spectral signature (Silva et al., 2008). However, the spectral signature of submerged aquatic vegetation is complicated by the effect of the water, which both absorbs and scatters light, as well as different bio-optical constituents (coloured dissolved organic matter and other suspended solids) present in the water column (Giardino et al., 2019; Kirk, 1983). A multitude of bio-optical algorithms exist to correct for the effects of the water column; therefore, it is still possible to isolate the reflectance of submerged marine macrophytes and use this information to map and differentiate between species (Giardino et al., 2012, 2019; Jay et al., 2017; Lyzenga, 1978; Maritorena et al., 1994; Reichstetter et al., 2015; Schalles, 2006; Spitzer & Dirks, 1987; Varunan & Shanmugam, 2020; Wicaksono et al., 2019; Wilson et al., 2020). To correct for effects of the water column, it is usually necessary to include depth and/or include known reference information, such as the reflectance of sandy bottom at various depths. These may be possible to acquire in some, but not all cases; therefore, the use of these algorithms is only applicable in the case where additional information is available.

Specific wavelengths, mainly in the visible range, have been shown to give the most information about submerged aquatic vegetation: the near-infrared, red, red edge, and green regions (Aswatha et al., 2018; Peñuelas et al., 1993; Rowan & Kalacska, 2021; Silva et al., 2008; Timmer et al., 2022). This is due to both plant pigment composition and photosynthetic efficiency and will vary depending on whether the vegetation is submerged, floating, or emergent (Peñuelas et al., 1993; Williams et al., 2003). Several narrower ranges are suitable for separating green from brown and red from brown algae, in addition to a region key to identifying eelgrass (510 to 528nm, 596 to 601nm, 596 to 656nm, 643 to 656nm, and 500 to 530nm) (Chao Rodríguez et al., 2017; O'Neill et al., 2011). The signal derived from submerged species will be significantly smaller compared to that of floating species (Peñuelas et al., 1993). Usually, both finger and sugar kelp are

submerged; thus, it is essential to test methods that isolate bottom reflectance through water column correction and/or include depth related information. It is also important to select sensors that have high spectral resolution across ranges known to give information about submerged aquatic vegetation to accurately map marine macrophytes, such as hyperspectral sensors.

1.2 Objectives

The objective of the thesis is to test the efficacy of PRISMA hyperspectral satellite imagery for mapping *Laminaria digitata* (finger kelp), *Saccharina latissima* (sugar kelp), and *Zostera marina* (eelgrass) using an area off the coast of Sheet Harbour, Nova Scotia, as a case study. We want to assess the accuracy of using a PRISMA hyperspectral satellite image to map these species overall, individually, and in comparison, to using a Landsat-9 multispectral satellite image. We also want to investigate the effects of several processing decisions on overall accuracy, including whether to combine sugar and finger kelp as a single kelp class, the inclusion of depth as a feature, and the application of a water column correction.

1.3 Thesis Format

This thesis is structured as a single journal article, and as such, the thesis introduction provides more detailed context for the article below, with some repetition. The references are given in APA Style 7th edition, while the structure is loosely based on remote sensing journals such as Remote Sensing of Environment and International Journal of Remote Sensing.

1.4 Drop Camera Survey Approach

To access in-situ (on-the-ground) data of marine macrophytes to support this thesis, it was necessary to perform a drop camera survey, as there were no existing datasets suitable for this application, either due to scope or number of samples. Drop camera surveys involve capturing underwater imagery of the benthos and are usually completed with access to expensive equipment and multi-person crews, usually involving a vessel with a motor and a heavy drop camera frame system. However, this thesis project was undertaken with a very limited budget and therefore required a lot of creativity when it came to the field sampling approach. It was determined that a two-person sea kayak would be the most affordable vessel, one that could be more easily transported than a motorboat and would only require two persons to operate. Given the challenging weather conditions that can occur in coastal Nova Scotia, this was an ambitious,

yet doable, choice for a drop camera survey in a nearshore environment, within 2km from shore. Then, given that most drop camera systems are deployed from a vessel much larger than a sea kayak, there were no commercially available drop camera systems that were suitable in size or budget. Therefore, it was determined that the only option was to design and build a custom drop camera frame. While this task veers far outside of the realm of a typical remote sensing project and into the waters of engineering, it was a task that was zealously accepted. With lots of help from some engineering friends and the uOttawa makerspace, a custom drop camera frame was designed and assembled by cutting steel and welding, among other things. The custom frame ended up working as the perfect instrument, after some on-the-fly adjustments at the field site. The 2-person kayak team also successfully covered all the planned sampling sites and more, paddling more than 110km in frigid coastal waters of Eastern Nova Scotia. While the weather conditions did prove challenging on many occasions, the drop camera survey was a successful adventure.

Chapter 2: Differentiating eelgrass (*Z. marina*), finger kelp (*L. digitata*), and sugar kelp (*S. latissima*) at the Eastern Shore Islands, Nova Scotia, using PRISMA hyperspectral satellite imagery

Neve Foreman[1], Anders Knudby[1]

[1]Department of Geography, Environment, and Geomatics, University of Ottawa

Abstract

Laminaria digitata (finger kelp), *Saccharina latissima* (sugar kelp), and *Zostera marina* (eelgrass) are three marine macrophytes whose habitats are known as blue carbon ecosystems due to their outstanding carbon sequestration capabilities. It is important to distinguish these species, as they have different suitable water temperature ranges, contribute to the blue carbon ecosystem in different ways, and are at threat due to climate change. All three species are found at the Eastern Shore Islands (ESI), Nova Scotia, an Area of Interest (AOI) for ecological and biological importance. Previous regional studies using multispectral satellite sensors were unsuccessful at differentiating eelgrass from brown algae, but a hyperspectral satellite sensor offers the high spectral resolution (hundreds of bands <15nm wide) that is needed for detecting

subtle differences between species. This study assessed the ability of PRISMA 30m spatial resolution hyperspectral satellite to map eelgrass, finger kelp, and sugar kelp using an area near Sheet Harbour, Nova Scotia, within the ESI AOI, as a study site. In July 2025, in-situ data was collected by drop camera survey to confirm absence or presence of target species then combined with the spectral information from a PRISMA image taken on August 7, 2025. The data was split into training and testing subsets, then, using over 400 spectral features, a 5-fold cross validation was applied through Random Forest (RF) Recursive Feature Elimination (RFE). Several different RF models were trained and tested on the PRISMA data using the reduced feature sets. Two models were also trained and tested using Landsat-9 multispectral satellite image from July 27, 2025, using a similar approach. We found a >10% increase in accuracy from using the PRISMA hyperspectral satellite image over the Landsat-9 image (up to 49.2% balanced accuracy compared to 36.0%). The two highest-performing PRISMA models both included depth information, either directly or through a correction to obtain bottom reflectance. This study represents an improvement in differentiating brown algae from eelgrass in the region; eelgrass habitat was predicted at up to 57% recall, and finger kelp habitat was predicted at up to 71% recall. Further studies should focus on better mapping sugar kelp (recall <5%), as the heterogeneity of species in this region likely affects the models' accuracy.

2.1 Introduction

Laminaria digitata (finger kelp), *Saccharina latissima* (sugar kelp), and *Zostera marina* (eelgrass) are three marine macrophytes whose habitats include the Eastern Shore Islands (ESI), Nova Scotia. The habitats of many marine macrophytes, including eelgrass and kelps, are known as blue carbon ecosystems due to their outstanding carbon sequestration capabilities. It is important to distinguish these species, as they are biologically distinct, and add value to the blue carbon ecosystem for different reasons (Bartsch et al., 2008). Eelgrass's contribution to carbon accumulation per unit area is up to 3 orders of magnitude higher than terrestrial soils, with seagrass environments accounting for up to 33% of total oceanic CO_2 uptake (Röhr et al., 2018). Additionally, kelp forests in Nova Scotia are estimated to sequester more carbon than eelgrass by ~1.3 orders of magnitude, largely due to the role of export of dissolved organic carbon and their large habitat area (Alongi, 2018; Krumhansl et al., 2026; Wright et al., 2022).

Climate change has already begun to have an adverse effect on coasts, with ocean warming causing the poleward migration of certain marine macrophytes. Finger kelp, a cold temperate kelp, sugar kelp, a cosmopolitan temperate/boreal kelp, and eelgrass, a temperate seagrass, all have different suitable water temperature ranges (Diehl et al., 2024; Niu et al., 2012; Wernberg et al., 2019). Finger and sugar kelp have already had significant habitat loss (Filbee-Dexter & Wernberg, 2018); eelgrass has experienced habitat loss in some areas but is projected to have habitat gain in other areas (Wilson & Lotze, 2019). Rising sea surface temperature (SST) is expected to continue under a 'business as usual' climate emissions scenario, and the ESI, within the Scotian Shelf Bioregion (SSB), are showing a 0.37-0.39ºC ± 0.06ºC per decade trend in rising SST (Chen et al., 2020; Thomas et al., 2017; Wilson et al., 2019b; Wong et al., 2018). Beyond rising SST, marine heat waves can also be detrimental to these species, leading to high rates of mortality in both eelgrass and kelps, and reduced growth of kelps (Bartsch et al., 2013; Drew, 1983; Filbee-Dexter et al., 2020; Jabbari et al., 2024). As eelgrass, sugar kelp, and finger kelp are all foundational species, providing habitat for juvenile fish and other species, the loss of populations causes negative changes at the ecosystem level (King et al., 2025; Wernberg et al., 2019).

Marine macrophytes, including finger kelp, sugar kelp and eelgrass, are spectrally distinct, allowing them to be identified by a satellite with sufficient spectral resolution (Fyfe, 2003; Schmidt & Skidmore, 2003). In principle, hyperspectral imagery is advantageous for mapping marine macrophytes as it has the potential to detect subtle differences in the species' reflectance spectra due to very high spectral resolution (hundreds of bands with bandwidths <15nm) (Giardino et al., 2019). There are many studies that have used either multispectral imagery, airborne hyperspectral imagery, or other sensors (such as lidar) to map marine macrophytes; however, fewer studies exist that utilize satellite hyperspectral imagery. While multispectral imagery has been used successfully for mapping marine macrophytes, little success has been achieved at species-level differentiation, but rather the focus has been on mapping by species groups, or mapping one individual species (Hogrefe et al., 2014; Lewis et al., 2023; Wilson et al., 2019a, 2020, 2022). Multispectral satellite data have been shown to be limited in their ability to distinguish seagrass from seaweed-dominated habitats in Atlantic Canada, and macroalgae is often misclassified as seagrass (Wicaksono et al., 2019; Wilson et al., 2020). Higher accuracy in detecting eelgrass in Western Canada was reported

using high spectral resolution airborne hyperspectral data compared to multispectral satellite imagery over the same area (O'Neill & Costa, 2013).

Submerged kelp has been successfully detected where there is a narrow peak in the red-edge band; however, given that all submerged vegetation has reflectance peaks at broadly similar wavelengths (red, red-edge, and green), hyperspectral imagery, with its additional spectral information, can be required to distinguish species or species groups (Rowan & Kalacska, 2021; Timmer et al., 2022). In the context of hyperspectral remote sensing, the availability of hyperspectral satellite data is relatively new, and such data are now more accessible than airborne hyperspectral imagery, presenting an opportunity for researchers to utilize hyperspectral data at little to no cost (Dierssen et al., 2021; Qian, 2022). Successful species-level differentiation, eelgrass detection, and submerged kelp detection have been achieved with the help of high spatial resolution airborne hyperspectral imagery, indicating the capability of hyperspectral sensors for distinguishing between species (Clarke et al., 2021; Marcello et al., 2018; O'Neill & Costa, 2013; Phinn et al., 2008; Uhl et al., 2016; Vahtmäe et al., 2020; Williams et al., 2003). Detection of seagrass patches using Hyperion satellite hyperspectral imagery has also been demonstrated, but differentiation of seagrass from other macrophytes, or between species of seagrass, was not attempted (Li et al., 2012).

Overall, many studies have used multispectral satellite imagery to map bottom habitats with some success, while a much smaller number of studies used hyperspectral imagery, and an even smaller number used hyperspectral satellite imagery. No study has successfully mapped bottom habitat in Atlantic Canada at the species-level, or even the subgroup level (i.e., brown algae) using hyperspectral satellite imagery. Both PRISMA and EnMAP hyperspectral satellites, new in the last 8 years, offer access to free hyperspectral satellite images (Loizzo et al., 2018; Storch et al., 2023). However, access currently requires requests to be submitted in advance, with a limited quota allocated to each user. Therefore, it remains to be seen whether any added benefit of using hyperspectral satellites outweighs the added inconvenience of limited data availability and preplanning, or other challenges such as dealing with a high-dimensionality dataset.

2.2 Study area

The research was conducted off the coast of Sheet Harbour, Nova Scotia, Canada, within the Eastern Shore Islands (ESI) Area of Interest (AOI). The ESI were identified as an AOI by the Department of Fisheries and Oceans (DFO) in February 2018, and cover a total approximate size of 2,000km^2. A marine AOI is defined as such when a criterion is met for biological and ecological importance in a unique geographical location (Department of Fisheries and Oceans Canada, 2024). One of the unique features of the study area is that the waters are colder relative to the other coastal waters of Nova Scotia, and the relatively cold temperature of the water of the region is expected to persist in the future, in contrast to other geographical areas, where oceans are expected to warm (Jeffery et al., 2020). This makes the area important to study as species of kelp adapted to colder temperatures, including *L. digitata* and *S. latissima*, are more likely to keep their current suitable habitat. Moreover, the Eastern Shore Islands have a diversity of macrophyte communities and a mix of subtidal substrate types. The site off the coast of Sheet Harbour was selected due to having known high populations of *L. digitata*, *S. latissima*, and *Z. marina*, which are the example species in this case study (Krumhansl et al., 2024). In previous field surveys, finger kelp was the dominant kelp species in this area, followed by sugar kelp, while eelgrass was dominant throughout the intertidal zone of the Eastern Shore Islands. While finger and sugar kelp often grow heterogeneously, in Nova Scotia, finger kelp tends to grow shallower than sugar kelp, mostly from 0 to 5m depth, while sugar kelp mostly grows from 5 to 20m depth (Adey & Hayek, 2011). Moreover, other marine macrophytes were present at the study site during sampling, which complicated the task of distinguishing the species of interest. The benthic habitat in this area was heterogeneous, according to both the literature and the field survey, with habitat patches that varied approximately every 400m, which is much smaller in comparison to other areas of Nova Scotia's coastline (Jeffery et al., 2020). Therefore, the area is suitable to test the use of hyperspectral imagery for mapping this heterogenous habitat. The shoreline type at the study site is mainly boulder/cobble beach or bank and is characterized by an irregular coastline with several small, rocky islands; this is an ideal habitat for kelps (Environment and Climate Change Canada, 2008). There was also sandy substrate in shallow areas, suitable for eelgrass. The study site off the coast of Sheet Harbour is small, approximately 40km^2, with ~13 km^2 covered by shallow coastal water <10m deep, to ensure that in-depth field surveys could be carried out by sea kayak, while also covering many potential patches of benthic habitat (see Figure 1).

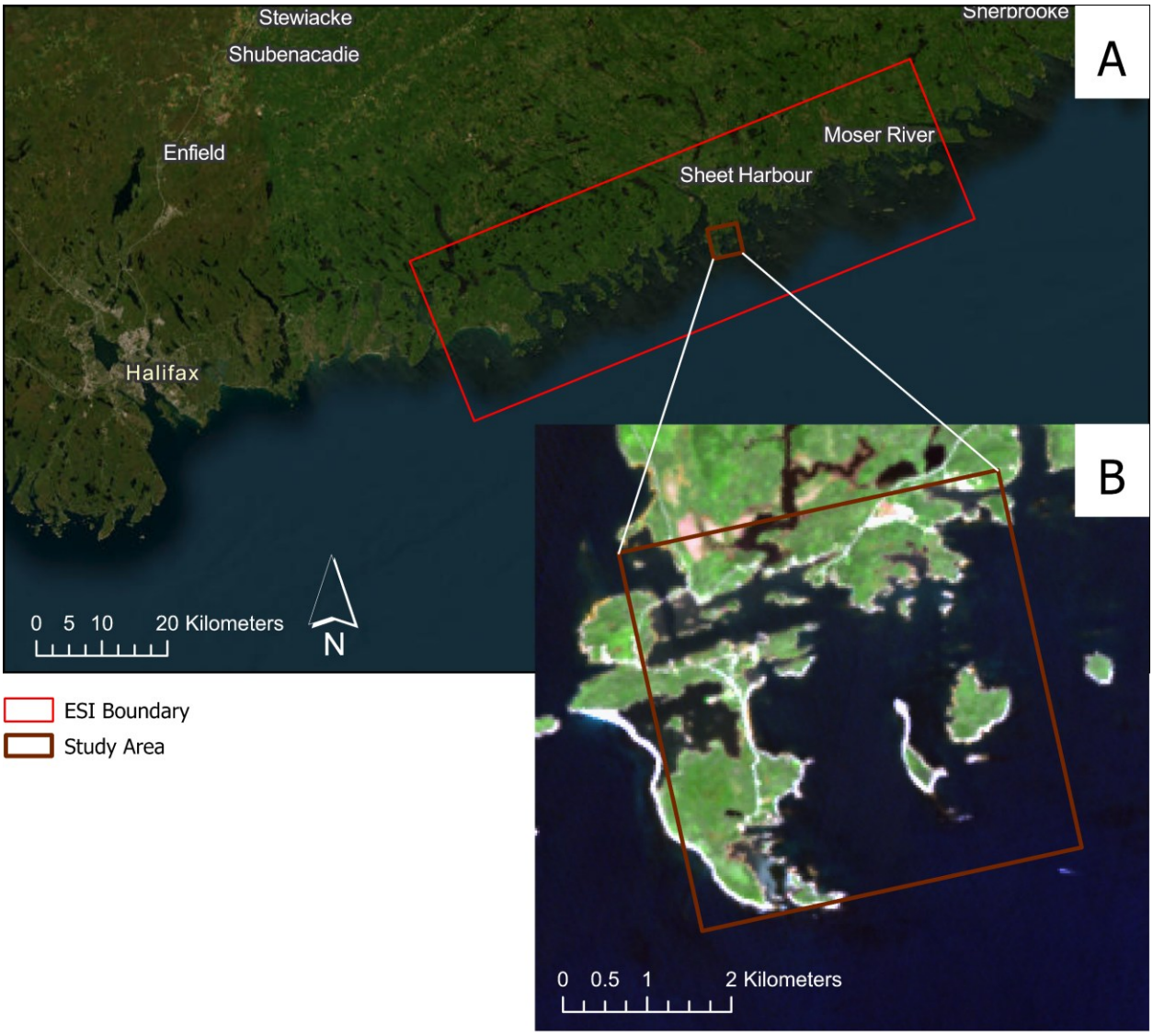


Figure 1. A: Small-scale map showing the approximate boundary of the ESI AOI in relation to Halifax, Nova Scotia, and the study site at Sheet Harbour. B: Large-scale map showing the study site, off the coast of Sheet Harbour.

2.3 Methodology

The overall methodology from in-situ data collection and image tasking to model evaluation is shown in Figure 2.

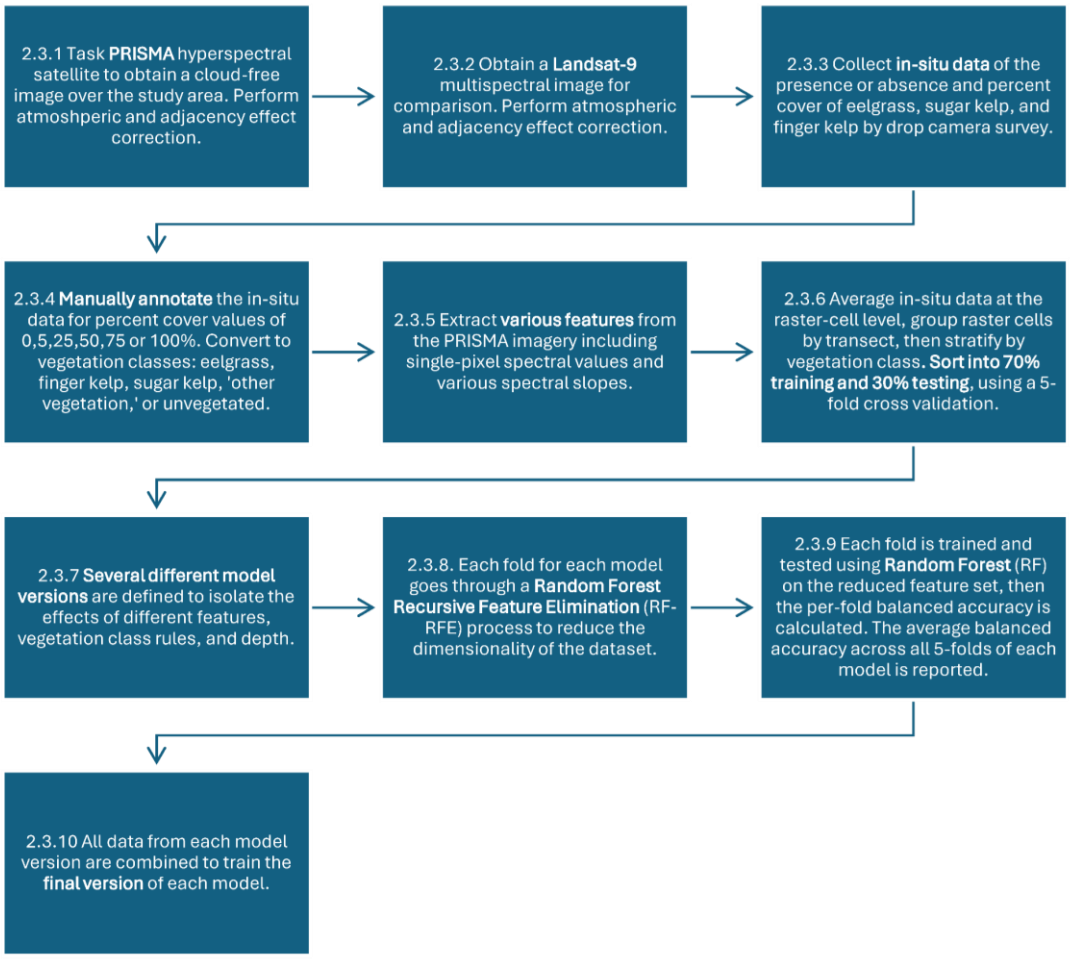


Figure 2. Flowchart outlining the process of in-situ and satellite data collection, processing, and training and testing. Each number corresponds to a section below that provides more details.

2.3.1 Hyperspectral satellite tasking and image processing

PRecursore IperSpettrale della Missione Applicative (PRISMA) hyperspectral satellite was tasked to obtain a cloud free image (<15% cloud cover) over the study area, as close as possible to the date of in-situ data collection, from May to September 2025. PRISMA has a very high spectral resolution with 250 bands <12nm wide covering a spectral range from 400-1010nm in the Visible and Near-InfraRed (VNIR) range and 920-2500nm in the SWIR (Short-Wave InfraRed) range (Loizzo et al., 2018). The satellite has a revisit frequency of 29 days and produces imagery with a spatial resolution of 30m. PRISMA provides different levels of data products, ranging from Top of Atmosphere reflectance products with minimal corrections to products that have undergone extensive preprocessing, including atmospheric correction, and conversion to surface reflectance.

Several observation requests were submitted to PRISMA to ensure that at least one image with little to no cloud cover over the study area was obtained.

The image used for the final classification task was chosen according to a variety of factors including the time of image capture, cloud coverage, haze, waves, and glint. Cloud coverage was the most important factor as it was necessary to select an image where as little as possible of the study area was obscured by cloud. Priority was also given to selecting an image taken closest to the time of field sampling, in late July 2025. The selected image was taken on August 7th, 2025, and was cloud free over the study area, taken at low to mean tide, within less than a month of the field sampling period. The image has minimal striping noise and appears to be of overall good quality, as observed from the single band image at 446nm (see Figure 3).

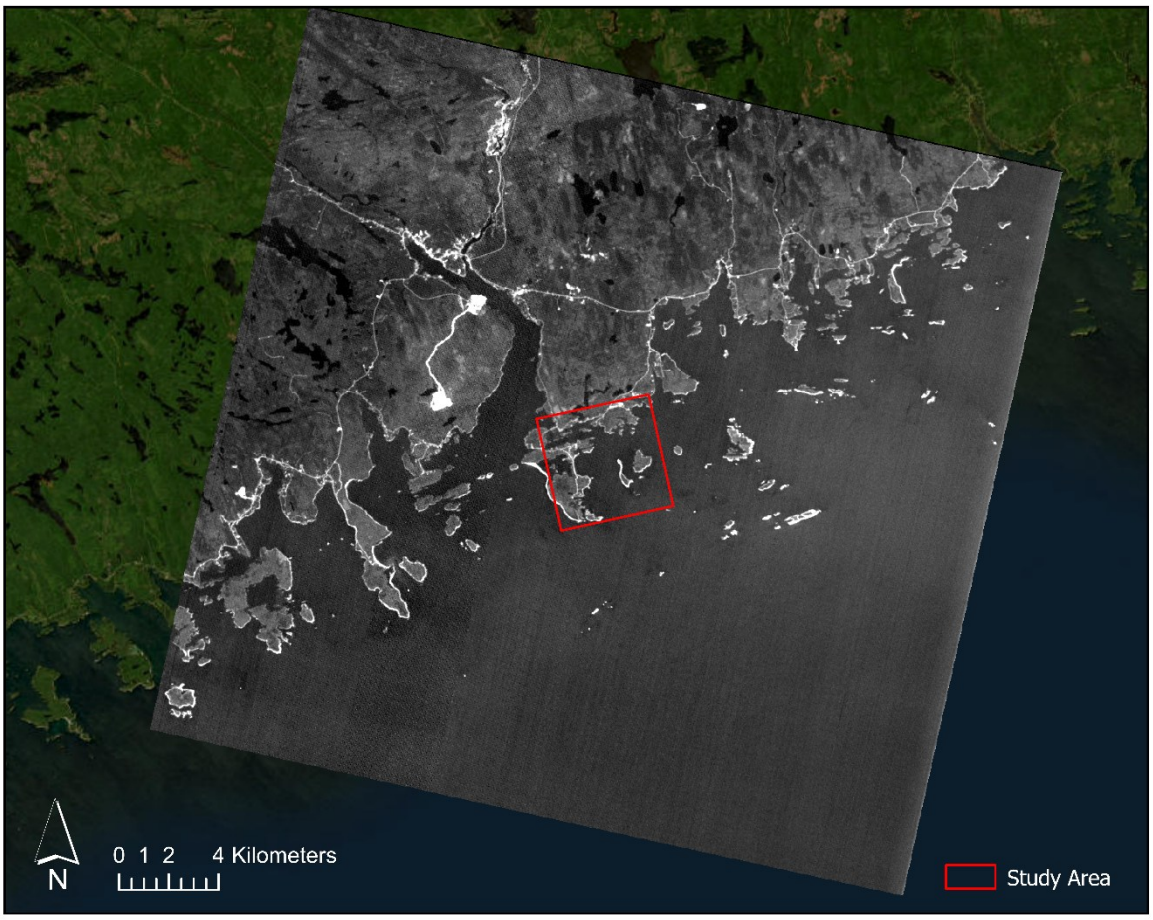


Figure 3. The 446nm from the PRISMA image acquired August 7th, 2025, shows overall good quality with some striping noise.

The Level 1 image was atmospherically corrected to a surface reflectance (rhos) product using ACOLITE, which performs well over coastal waters (He et al., 2024; Vanhellemont, 2019). Moreover, we used T-Mart (Wu et al., 2023) to correct for the adjacency effect. The PRISMA image was georeferenced according to a Landsat-9 image in ArcGIS Pro using control points at well defined features, such as island points, as Landsat-8/9 has better geolocation accuracy than PRISMA (Choate et al., 2023; Kim et al., 2022).

2.3.2 Multispectral image acquisition and processing

A Landsat-9 multispectral satellite image was also acquired for comparison purposes (see Figure 4). Landsat-9 has a spatial resolution of 30m with 7 standard spectral bands across the visible, near-infrared, and shortwave-infrared regions (Masek et al., 2020). The image, from July 27th, 2025, is cloud free over the study area besides some possible cirrus cloud contamination and shows good details of the bottom. It shows no obvious striping or other noise. A Landsat-9 image was selected over other multispectral satellite sensors as it has the same spatial resolution as the PRISMA image (30m), allowing a comparison to be focused on spectral resolution without influence from differences in spatial resolution. The Landsat-9 image was atmospherically, and adjacency effect corrected using the same software as the PRISMA image, ACOLITE and T-Mart (Vanhellemont, 2019; Wu et al., 2023). Bands 9 – cirrus detection band – and 8 – panchromatic band – were not included, only bands 1-7 were used.

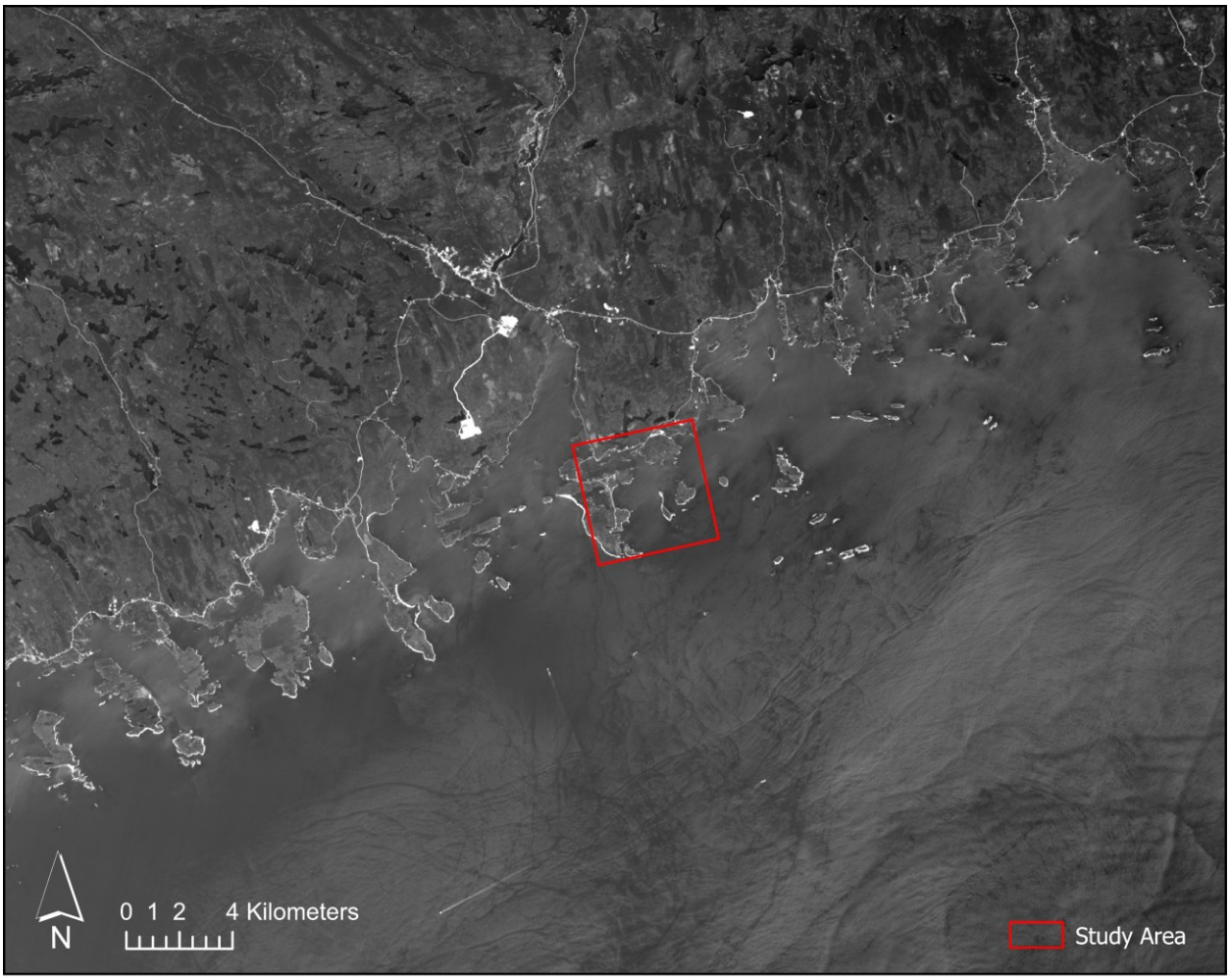


Figure 4. Landsat-9 image, single band (blue: 450-510nm), no visible striping noise.

2.3.3 In-situ data collection

In-situ data were collected across the study site to confirm the presence or absence and percent cover of eelgrass, sugar kelp, and finger kelp. A drop camera survey method was used across all depths from 0.5 metres above Chart Datum (CD) to 12 metres below CD according to Canadian Hydrographic Service Non-Navigational (CHS NONNA) bathymetric data (Canadian Hydrographic Service, 2025a). Drop camera target points were created in a Geographic Information System (GIS) platform, then embedded into a Garmin Global Positioning System (GPS) Map 64S device. Sampling points were determined according to a systematic sampling pattern at all center points of a 500m grid across the study area oriented parallel to the dominant coastline shape (see Figure 5). Points falling on water-covered areas up to 12m depth were included initially. Then, points closer than 100m to shore were moved to at least 100m and less than 150m

away from shore (Environment and Climate Change Canada, 2008). Moreover, points were added where large gaps existed due to irregularity of the shoreline, such as small cove areas or narrow areas between islands, or where points fell just outside of the depth perimeter. Some additional points were also added during sampling, where an opportunity allowed the extra point to be taken (see Figure 5). Inland water areas (i.e., lakes, rivers, or saltwater ponds) were not included in the survey. After sampling, a depth threshold of 10m was applied to exclude optically deep water (ODW).

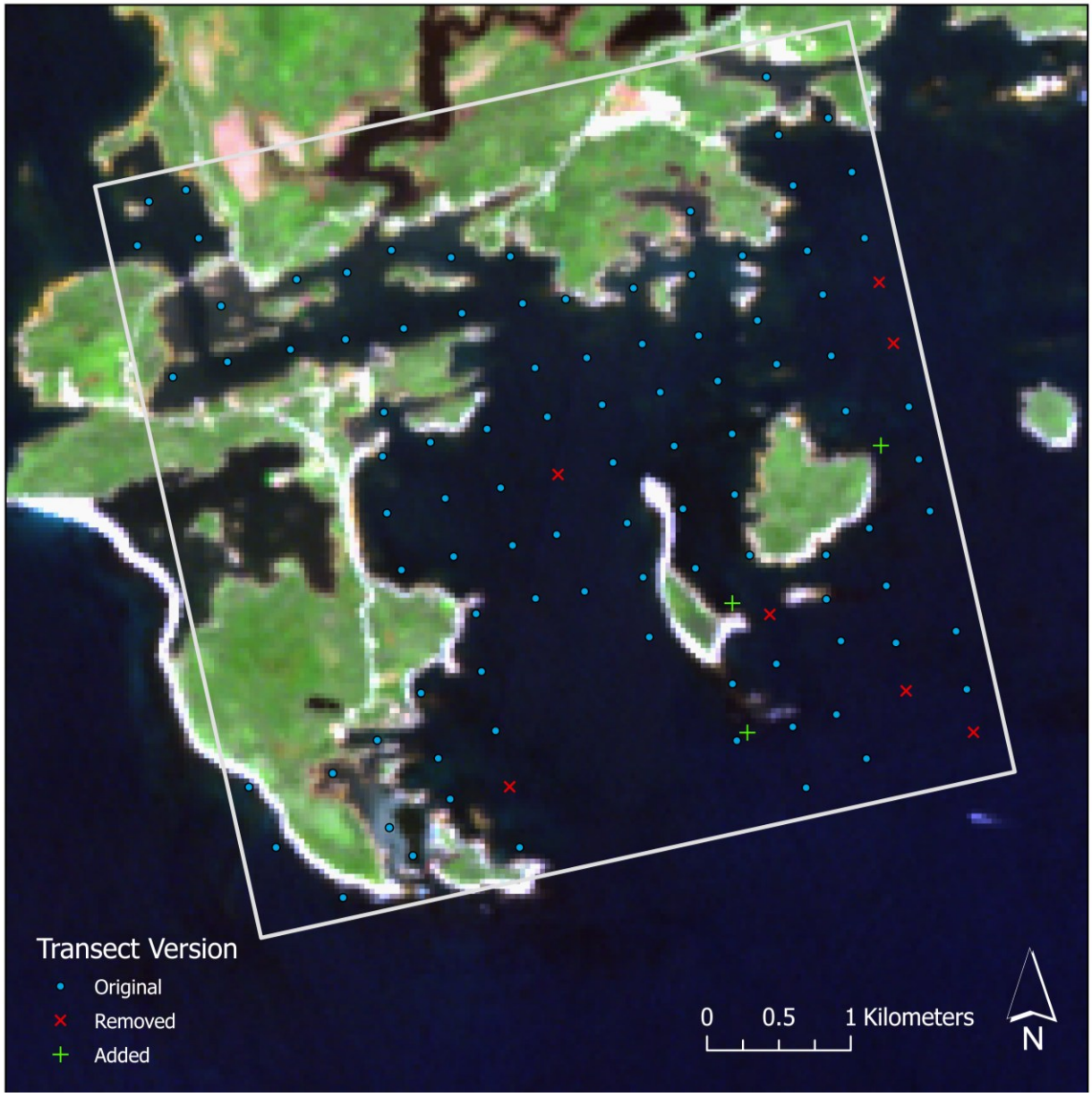


Figure 5. Drop camera survey sampling point scheme near Sheet Harbour, NS. Each point corresponds to a location where a 3-minute video was taken.

The camera used in the drop camera system was a GoPro Hero 11 Black attached to a custom-built steel drop frame (see Figure 6). The drop frame was designed to be lightweight and compact yet have sufficient mass to minimize tilting during sampling. The frame is a 0.375 x 0.375m square towed by rope with 4 connection points on the frame, leading to an anchor shackle. Two diving lights, positioned on either side of the camera, are directed downwards towards the centre of the frame to ensure that any vegetation below is visible and can be easily identified. The drop frame was towed approximately 1-2m above the bottom, as estimated with reference to the CHS NONNA bathymetric data (Canadian Hydrographic Service, 2025a) and by dropping the frame to the bottom in some cases to estimate the bottom depth before raising the frame to the appropriate height. The average predicted tidal range at Sheet Harbour during the field sampling dates was ~1.4m (Canadian Hydrographic Service, 2025b); therefore, it was possible to sample points above CD (up to 0.5m) at high tide.

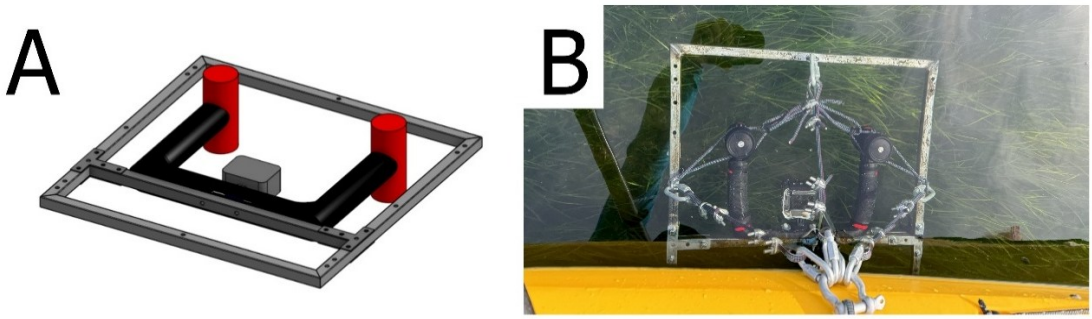


Figure 6. A: Drop camera frame design prior to attaching rope. B: Drop camera frame during deployment.

The boat used for the survey was the Wave Sport Horizon 160T + rudder tandem kayak (see Figure 28), chosen due to its ability to access very shallow waters, store equipment, and provide stability in choppy waters. Equipment was stowed in the bow and stern storage hatches during sampling or attached to the top of the boat. The survey was conducted by two people: the person at the front of the kayak was responsible for navigating to the drop camera points and deploying the drop camera frame, while the person at the back was responsible for steering, maintaining boat stability during instrument deployment, and recording GPS waypoints at the beginning and end of each 3-minute interval. After navigating to each point, diving lights and

camera were turned on, recording was started, then the drop frame was lowered to the appropriate height of approximately 1-2m above the bottom, or 1m above the canopy of the dominant vegetation, if visible. After being lowered, 3 minutes of video footage were recorded while allowing the kayak to drift.

2.3.4 In-situ data annotation

After the survey, the 3-minute interval for each drop camera video was calculated by stopping the video one second before the frame was lifted back up and calculating the 3-minute interval backwards from that stopping point (as visually observed in the video). Still shots were extracted from the video footage at thirty-second intervals, for a total of 7 still shots per 3-minute video, then each frame was assessed for the presence or absence and percent cover of eelgrass, sugar kelp, and finger kelp (see Figure 7). Percent cover was registered in bins of <5% cover, 6-25% cover, 26-50% cover, 51-75% cover, and 76-100% cover (Hogrefe et al., 2014). Each still shot was imported into a photo editing software, and a grid was overlayed, separating the photo into four quadrants (see Figure 8). Then, each quadrant was given an estimated value of 0, 5, 25, 50, 75, or 100% cover of each species by visual estimation, and the average value of all four quadrants was calculated and the observation attributed to the correct bin. Due to rounding, the total percent cover values may not sum to 100%.

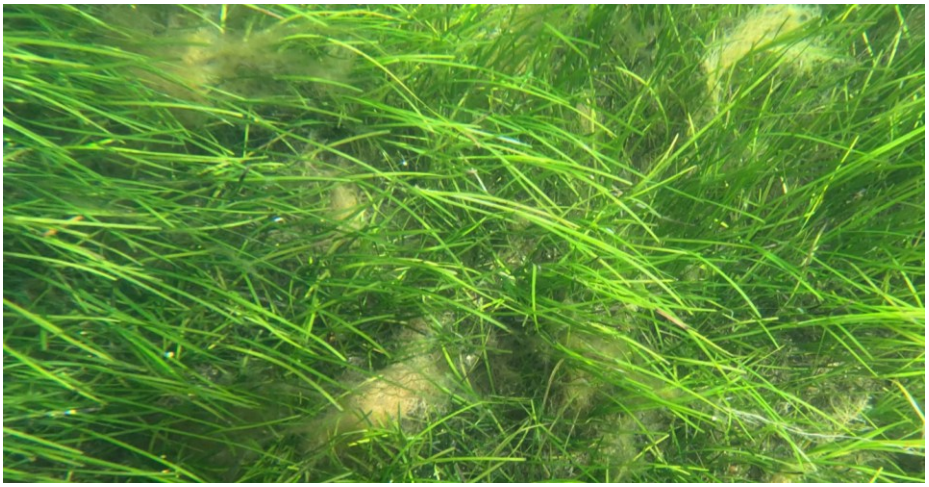
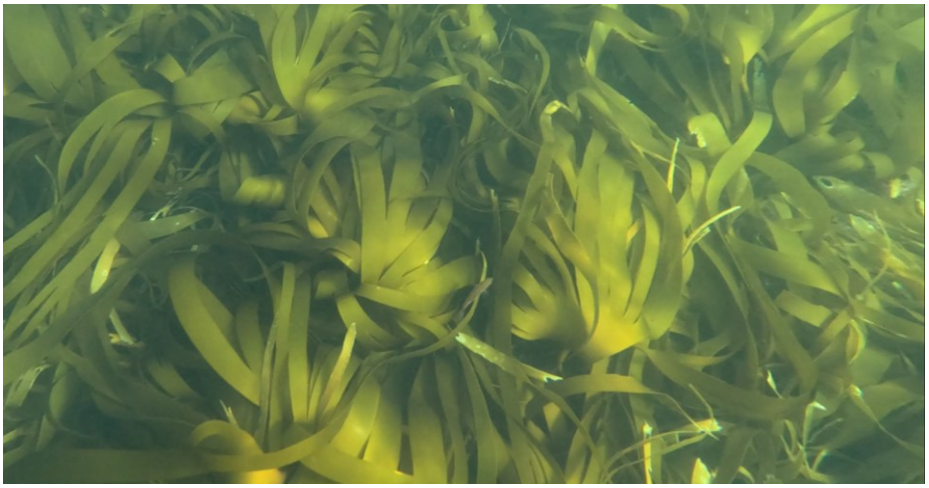
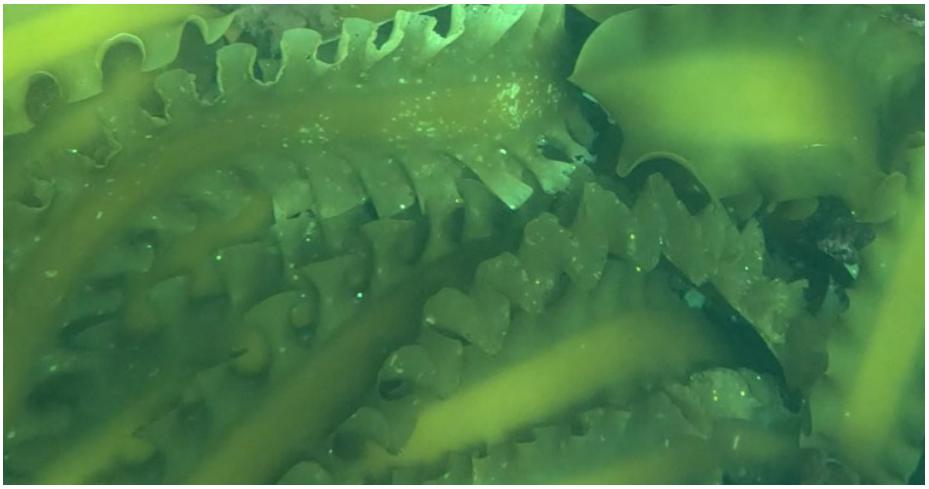
Species	Sample
Zostera marina (eelgrass)	
Laminaria digitata (finger kelp)	
Saccharina latissima (sugar kelp)	

Figure 7. Examples of the three target species: eelgrass, finger kelp, and sugar kelp.



Figure 8. Example of photo for annotation. This photo, M6-1, was annotated with 25% sugar kelp, 0% eelgrass, 5% finger kelp, and 75% other vegetation.

In situations where any photo was too unclear to assess percent cover (due to being blurry or too close to the bottom), the point was removed from the dataset. In situations where the photo was taken at the point during the video (usually at approximately 90 seconds) where the camera depth was re-adjusted (and therefore the photo was unclear), the image was replaced with a photo right before or after the camera hit the bottom during readjustment, up to 5 seconds before or after the time the photo was meant to be sampled from. In some situations, the video was played back to assist in identifying species. A straight line between the two GPS points marking the start and end of the 3-minute videos was used to estimate the path of the kayak during sampling. Then, points were created along this line at evenly spaced intervals and matched to the annotated images.

Vegetation classes were assigned using percent cover values for eelgrass, finger kelp, sugar kelp, 'other vegetation,' and unvegetated. A threshold of 40% was used: whichever vegetation type exceeded this threshold with the highest percent cover was designated as the class. If total vegetation cover across all species was below 40%, the class was labeled unvegetated. If no single species surpassed the threshold but two species together did, the class was designated as mixed. A set of 100 ODW points was created by visual assessment using areas within or nearby to the study

site, to create a reference to show the similarities and differences between ODW and all species' reflectance spectra (see section 2.4.1).

A land mask was derived by manual threshold according to the contrast between land and water at 1009nm, at a pixel value of 0.06. Any in-situ data points falling over land (usually due to being very close to shore or drifting closer to shore during sampling) were removed from the dataset, and no predictions were performed over land.

2.3.5 Machine learning features from PRISMA imagery

The machine learning features included the single-pixel spectral values from the hyperspectral bands, the distance from land, the spectral slope across each adjacent band pair, the spectral slope across every other band pair (e.g. the slope across band 407nm, 416nm, and 424nm), and in some cases, the mean CHS NONNA depth (Canadian Hydrographic Service, 2025a). Several spectral slopes identified from the literature were also used, including an 'eelgrass specific' slope (500 to 530nm), suitable intervals for separating green from brown and red from brown algae (510 to 528nm, 596 to 601nm, 596 to 656nm, and 643 to 656nm), the local reflectance maxima for all phaeophytes (700 to 2500nm), and the near-infrared, red-edge, and green ranges (620 to 750nm, 680 to 750nm, and 500 to 578nm) (Aswatha et al., 2018; Chao Rodríguez et al., 2017; O'Neill et al., 2011; Timmer et al., 2022). In most cases, the single-pixel spectral values were ACOLITE and adjacency effect corrected at-surface reflectance; however, one model version used estimated bottom reflectance, corrected using 93 unvegetated pixels from the regular dataset at different depths, the NONNA depth values, and 100 ODW pixels from within or next to the study site (Maritorena et al., 1994).

2.3.6 Dataset size, sorting, and machine learning process

The overall data sorting process, manual 5-fold cross validation split, RF-RFE, and model training process is shown in Figure 9. First, the percent cover (benthic class) values derived from the in-situ data were averaged at the raster cell level. The total size of the full regular dataset after averaging in-situ points was 267 raster cells. Other vegetation and unvegetated are the most dominant classes, making up ~75% of the total dataset together, and both kelps, eelgrass, and mixed vegetation are the smallest classes (see Table 1). Then, the data was stratified according to vegetation class (unvegetated, finger kelp, sugar kelp, eelgrass, 'other

vegetation,' or mixed vegetation) at the transect level, rather than the cell level, to reduce spatial autocorrelation. Then, the data was split into 5-folds, each with a unique and random 70% training and 30% testing split. As such, the split of each of the five folds was not exactly 70% training to 30% testing as the transects had a differing number of corresponding raster cells (e.g. Fold 4 was 66.47% training and 33.53% testing). After splitting, each fold went through a separate process of RF-RFE, followed by a separate process of training and testing. The balanced accuracy scores from training and testing were averaged across all 5-folds to generate an average balanced accuracy score for each model.

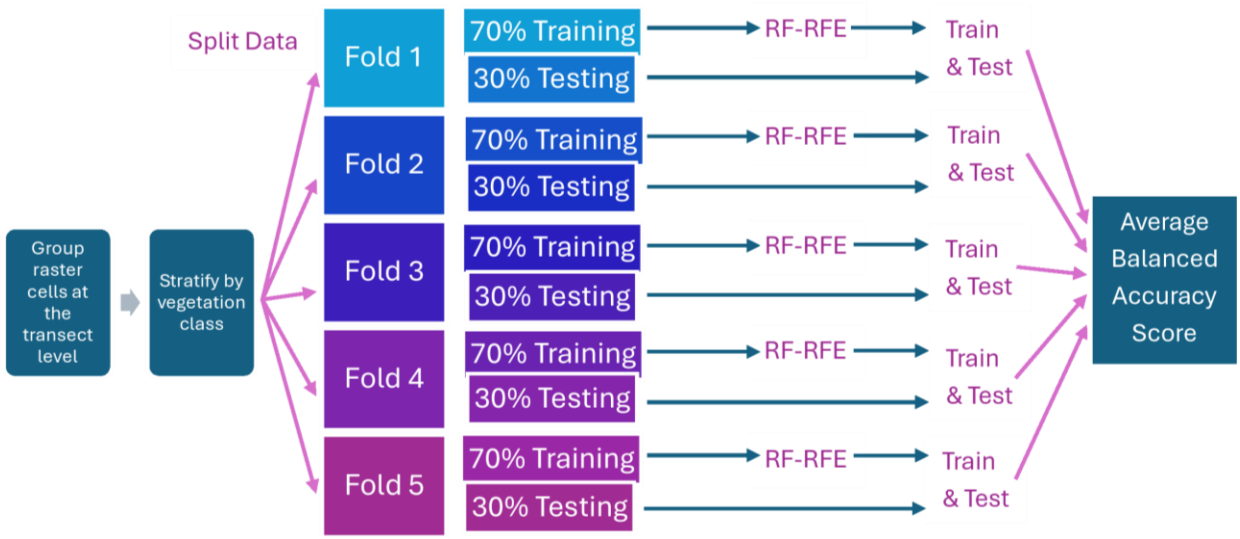


Figure 9. Data sorting and machine learning process flowchart. Further details on Random Forest Recursive Feature Elimination (RF-RFE) and model training can be found in sections 2.3.8 and 2.3.9. Each fold has an approximate, not exact, 70% to 30% split.

Table 1. Size (# of raster cells) of each class for the standard vegetation class rule (10m depth threshold).

Class	# of raster cells
Finger Kelp	12
Other vegetation	80
Sugar kelp	15
Eelgrass	11

Unvegetated	120
Mixed Vegetation	29

2.3.7 Random forest model definitions

Several different model versions were defined to isolate the effects of different features, vegetation class rules, and depth (see Table 2). First, the basic version of each model was created: model R, the PRISMA model with all PRISMA features, and model L9, the Landsat-9 model. Next, depth was simply added as a predictor to each of those models to create the RD and L9D models. Then, a model that estimates bottom reflectance from PRISMA at-surface reflectance, model M, was created, using various unvegetated pixels and depth to apply a correction (Maritorena et al., 1994). A conservative depth model was created from the PRISMA feature set to test shallower waters, only up to 5m depth, called the 5m model, which has a total size of 167 raster cells. Finally, the kelp model, K, was created, that combines both finger and sugar kelp into a single class, and model KD, with depth added as a predictor, both based on the PRISMA features.

Table 2. Description of all models used and their features.

Model Name	**Definition**	**Number of Vegetation Classes**	**Input Features**
R	"Regular" model version with all PRISMA features	6 (Finger kelp, sugar kelp, eelgrass, other vegetation, mixed vegetation, unvegetated)	**469 features** including **at-surface reflectance** values for each band, **spectral slopes** (adjacent and 1 apart band pairs), **distance from land**
RD	"Regular" model version, but with depth added as a predictor	6	469 features + **depth** = **470 features**

M	"Maritorena" model, where PRISMA at-surface reflectance values were corrected to estimate bottom reflectance (Maritorena et al., 1994)	6	469 features; values for each band represent **bottom reflectance** rather than at-surface reflectance
5m	5m is considered the threshold for deep water rather than 10m	6	469 features
K	"Kelp" model version where both kelps (sugar and finger kelp) are grouped into a single 'kelp' class	5: kelp, eelgrass, other vegetation, mixed vegetation, unvegetated	469 features
KD	"Kelp" model version, but with depth added as a predictor	5	469 features + **depth** = **470 features**
L9	"Landsat-9" model version with all Landsat-9 features	6	**8 features**: 7 surface reflectance bands as predictors (at 430-450nm, 450-510nm, 530-590nm, 640-670nm, 850-880nm, 1570-1650nm, and 2110-2290nm), and distance from land
L9D	"Landsat-9" model version, but with depth added as a predictor	6	8 Landsat-9 features + **depth** = **10 features**

2.3.8 Machine learning feature reduction

A feature reduction step was required to reduce the dimensionality of the hyperspectral dataset prior to final classification (Hughes, 1968; Keogh & Mueen, 2017). We used a supervised wrapper feature selection technique, where the features are selected according to their classification accuracy during a preliminary supervised classification test (Benediktsson & Ghamisi, 2015; Maldonado & Weber, 2009; Pal & Foody, 2010; Poona et al., 2016). Specifically, we used the Random Forest Recursive Feature Elimination (RF-RFE) technique, which has been proven effective in selecting important spectral bands for hyperspectral classification and is desirable due to its ease of implementation compared to other feature selection techniques (Adam et al., 2012; Granitto et al., 2006; Pullanagari et al., 2018).

RF-RFE was implemented in Python using RandomForestClassifier and GridSearchCV from the Scikit-learn Python package, with balanced accuracy as the selection metric (Pedregosa et al., 2011). The grid to select the best parameters included the following values: *n_estimators*: 100, 200, 300, 500, 800, or 1000, *max_depth*: None, 10, 20 or 30, *max_features*: sqrt or log2, *min_samples_split*: 2, 5 or 10, and *min_samples_leaf*: 1, 2 or 4. Weights were also used to balance between classes as the vegetation classes were all minority classes. During the feature elimination, a step size of 10 features was used to eliminate at each round, with a minimum number of 10 features in the resulting reduced feature set. Each fold underwent RF-RFE separately, resulting in a unique reduced feature set.

2.3.9 Machine learning model training and evaluation

For model training, a Random Forest (RF) machine learning classifier was employed (Breiman, 2001). Random forest was selected as it is easy to implement and shows good performance in studies (Belgiu & Drăgu, 2016; Sarker, 2021). The classifier was implemented using RandomForestClassifier from the SciKit-learn Python package (Pedregosa et al., 2011). The tuning process to select the best parameters used the same grid as during the RF-RFE process (see section 2.3.8). Using the set of reduced features defined during the RF-RFE stage, each fold was trained and tested independently and evaluated for balanced accuracy. Then, the balanced accuracy scores of all 5-folds for each model were averaged to determine the average balanced accuracy for each model. Matthews correlation coefficient (MCC) was also reported as a secondary metric but not used directly for any evaluation.

2.3.10 Final model training

After evaluation, all the data were combined to train the final version of each model. The data were processed once again through RF-RFE, then the final model was trained using the best resulting feature set according to the internal balanced accuracy scores during the RF-RFE process and saved. The final models could then be used to generate predicted class maps, class probability maps or other outputs.

2.4 Results

2.4.1 Drop camera survey

Over 100 different camera drops were successfully completed across the study area, and several patterns were observed from the drop camera survey alone. Firstly, results were consistent with previous studies suggesting that kelp and other marine macrophytes grow heterogeneously in the region (Krumhansl et al., 2024) (see Figure 11); particularly, finger and sugar kelp were growing heterogeneously at 15 out of 40 transects (see Figure 10). Additionally, other macroalgae were present besides the species of interest, such as *Ceramium rubrum* (a red alga), *Codium fragile* (an invasive green alga), and *Saccorhiza dermatodea* (a brown alga) (see Appendix). *Fucus distichus* (rockweed) was consistently observed in the intertidal zone throughout the study area.

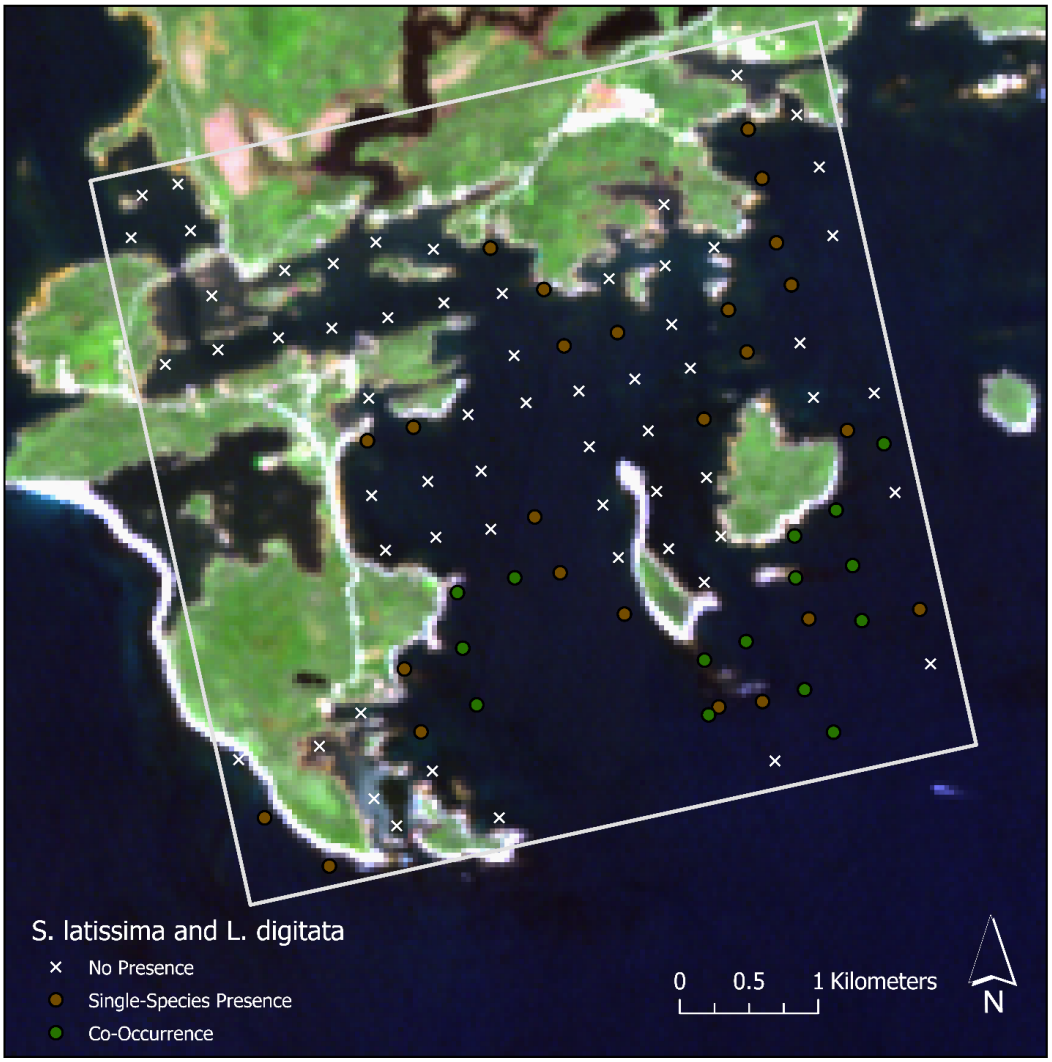


Figure 10. Heterogeneity (co-occurrence) of sugar kelp and finger kelp (>5% percent cover of each species).

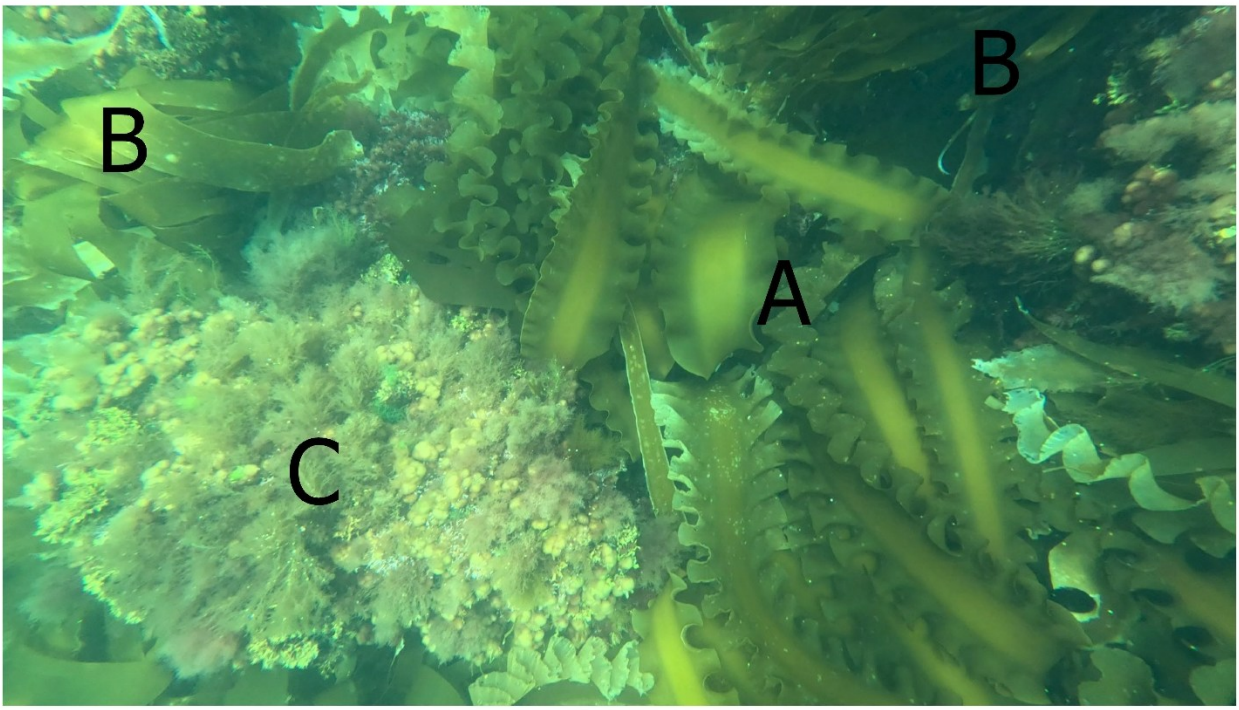


Figure 11. Still shot from the drop camera survey demonstrating heterogeneity between species. A: sugar kelp, B: finger kelp, and C: 'other vegetation.'

The average reflectance spectra from the in-situ data of all species showed similarities (see Figure 12). Notably, the average line of ODW was quite similar to some vegetation classes, particularly, the spectral signature of finger kelp and ODW were quite similar. However, there were still subtle differences in the spectral signatures that can be distinguished with the high spectral resolution that the PRISMA image provides. For example, at approximately 455nm, most classes experience a local peak, but with different slope degrees surrounding the peak, and eelgrass is the only species which does not peak there, even though its reflectance value is similar to the others (Figure 12). Similarly, at approximately 550nm and 600nm, all species experience a peak, but the degree of each differs subtly.

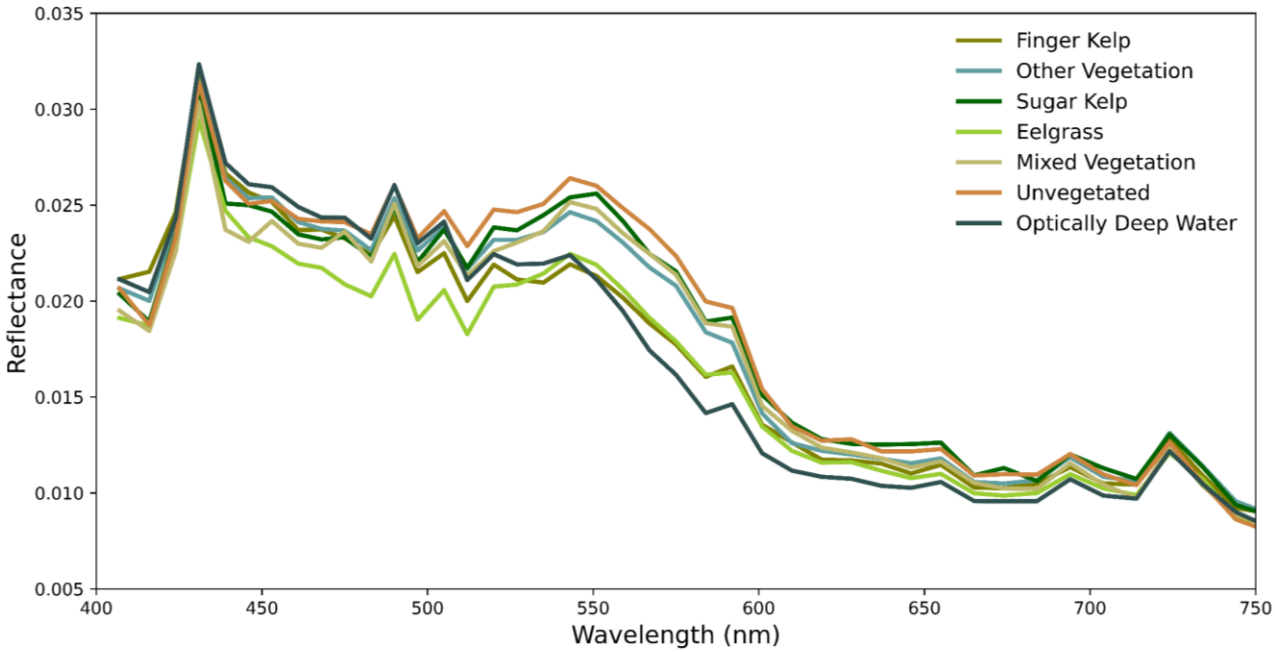


Figure 12. Average line of the spectral signatures of each class, in addition to optically deep water, derived from all admissible data (less than or equal to 10m depth) and the PRISMA single band values across the visible spectrum.

2.4.2 Feature elimination

Table 3 lists commonly retained features during the feature elimination process, across all standard PRISMA model versions. Both spectral slopes and unique band values were commonly retained, with ~68% band features and ~32% slope features among the top features selected.

Table 3. Top features selected - in 60% or more of PRISMA models' folds (excluding models K and KD).

Feature(s)	Retained in # of folds	Retained in % of folds
slope 2143 to 2151nm, slope 520 to 535nm	25	100
slope 2127 to 2143nm, band 512nm, band 527nm	23	92
band 535nm	21	84
band 497nm, band 1196nm, band 567nm	20	80

band 505nm	19	76
band 559nm, band 1240nm, slope 500 to 530nm, band 543nm, band 551nm	18	72
slope 520 to 527nm, band 461nm	17	68
slope 620 to 750nm	16	64
band 2143nm, slope 724 to 734nm, band 475nm, band 871nm	15	60

Out of the top 22 features, 14 were found in the visible range, 5 in the SWIR range, 2 in NIR range, and one slope covering both visible and NIR range (see Figure 13). Given that several SWIR features were selected, it is possible that this could be both from the species of interest (particularly eelgrass) or other species (particularly rockweed) in the intertidal zone that were sometimes emergent. As expected, many of the most important features were found in the visible range, as that is where reflectance peaks for aquatic vegetation occur and the range that best penetrates water (see section 1.1.3). Several of the most important features overlapped with Landsat-9 bands, while others were found between Landsat-9 visible bands, such as between Landsat-9 bands 2 and 3, suggesting added benefit of the additional bands produced by PRISMA.

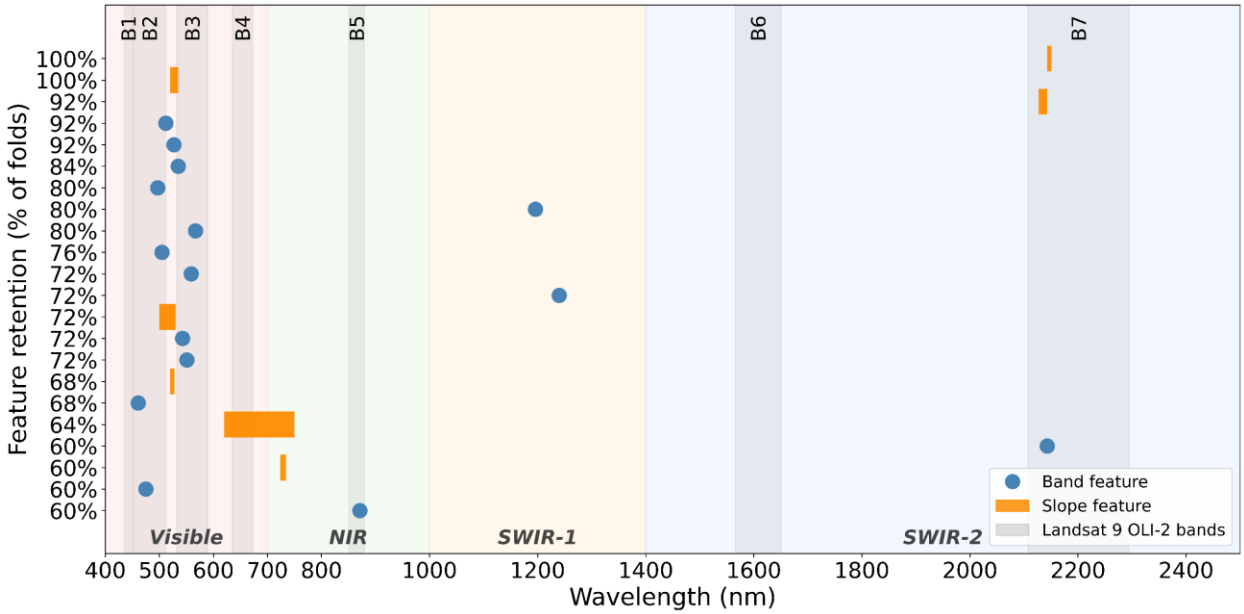


Figure 13. Shows the distribution of the most frequently selected PRISMA features (retained in 60% or more folds, excluding K and KD) across the spectrum of light and in relation to the relevant Landsat-9 OLI-2 bands.

The full RF-RFE process reveals how cross-validated balanced accuracy changes as features are progressively removed. Using model M as an example, we can see that both MCC and balanced accuracy grow when removing features, peaking at 70 features, then roughly stabilizing (see Figure 14). The growth is not very smooth, likely due to having a small data set.

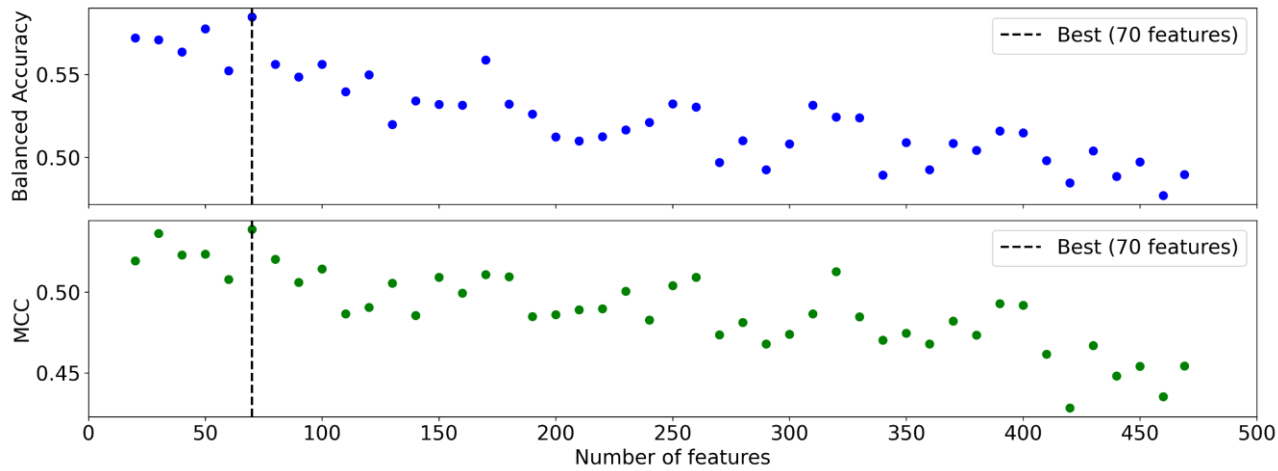


Figure 14. Feature elimination plot from full model M including balanced accuracy and MCC. Feature elimination proceeds iteratively from right to left in these plots.

2.4.3 Machine learning model results

The average accuracy of each machine learning model, across the five folds, is shown in Table 4. The two highest performing models were both PRISMA models that incorporated depth information, either directly (RD) or through an estimated correction for bottom reflectance (M). The highest performing PRISMA models were over 10% more accurate than the Landsat-9 models, showing the utility of incorporating more spectral information. Combining finger and sugar kelp into a single kelp class did not prove to be useful, as both kelp models (K and KD) performed the worst out of all PRISMA classes. The Landsat-9 models had the lowest balanced accuracy and MCC. There was an average ~5% improvement in accuracy after applying the adjacency effect correction compared to an initial round where only the atmospheric correction was applied.

Table 4. Model results summary.

Model	Balanced Accuracy (%)	MCC (-1 to +1)
R	47.0	**+0.45**
RD	**49.2**	+0.44
M	**48.1**	**+0.48**
5m	47.3	+0.39
K	39.7	+0.38
KD	41.5	+0.40
L9	**36.0**	**+0.36**
L9D	**33.6**	**+0.34**

The confusion matrices of the top two models, RD and M, show the models' strengths and weaknesses at predicting specific classes (see Figure 15). Model M had better recall of finger

kelp compared to model RD, where many finger kelp areas were misclassified as ‘other vegetation.’ While model RD showed higher overall accuracy, model M shows better recall values for not just finger kelp, but also of sugar kelp and unvegetated classes. However, both models show very poor recall of sugar kelp; in most cases sugar kelp was misclassified as ‘other vegetation’ or unvegetated.

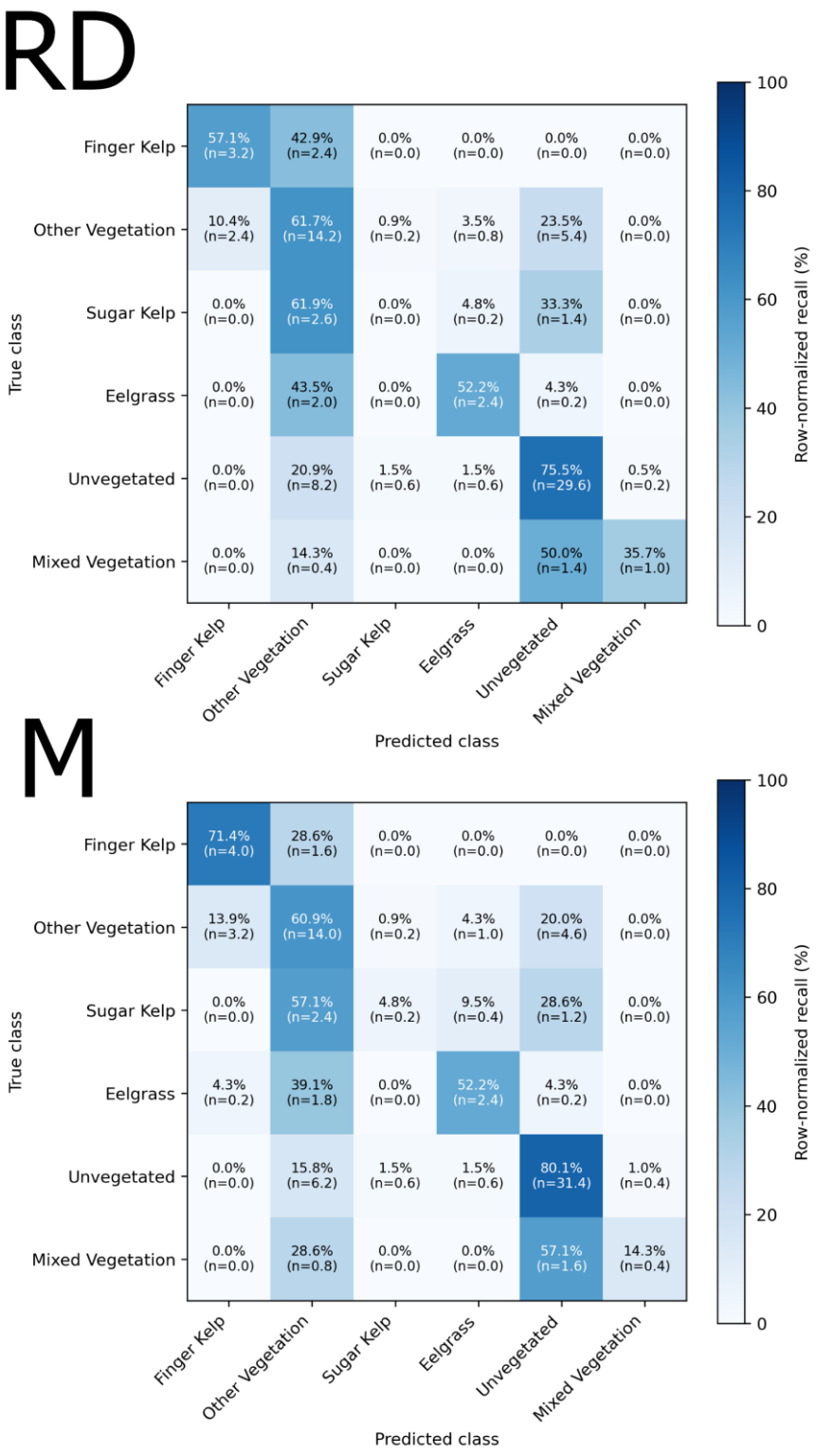


Figure 15. Confusion matrices of models RD and M as averages of all 5-folds during the testing stage. Row-normalized as the values were averaged across all 5-folds of the training and testing stage.

The output prediction map of RD (see Figure 16) identified several habitat patches, including eelgrass patches (A), and finger kelp patches (B). There are very few areas predicted as sugar kelp, which is consistent with the model's poor recall of that class. Moreover, there is a strip predicted as 'other vegetation' around the shoreline, which is consistent with the local habitat which is mainly *Fucus* (see Figure 23) at the intertidal zone throughout. After applying the adjacency effect correction, the 'other vegetation' surrounding the shoreline became more defined, and the overall accuracy of models increased by 5%.

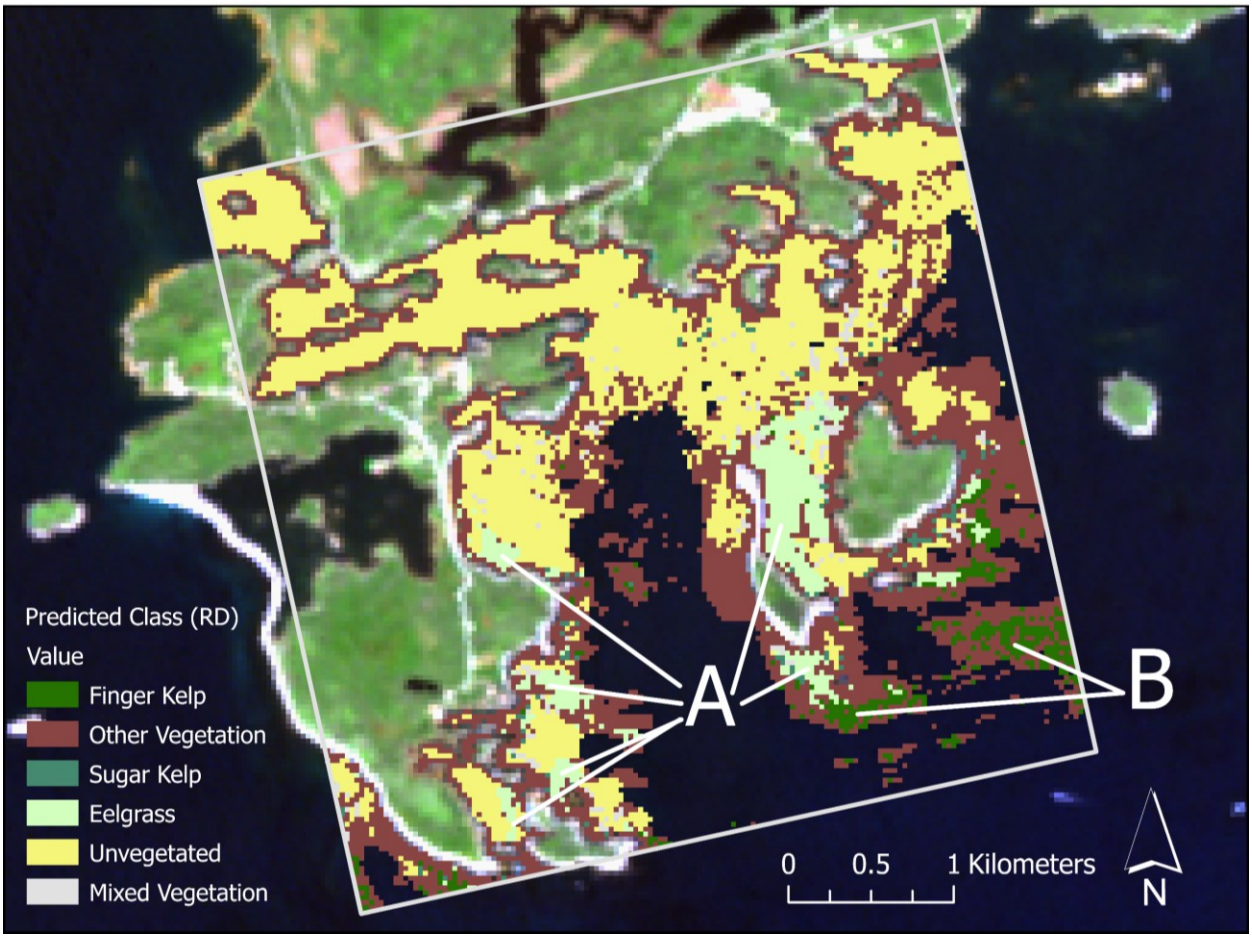


Figure 16. Output classification map from the highest performing model, RD. A: locations of identified eelgrass patches; B: locations of identified finger kelp habitat.

Knowing that model M has the highest recall of the finger kelp class, we generated a finger kelp probability map to help estimate finger kelp habitat (see Figure 17). The largest estimated patch with a high percentage of finger kelp was located at the south-east corner of the study area.

Predicted probability maps are useful to map the distribution of individual classes and may flag species presence even in areas with a lower percentage cover of the target species.

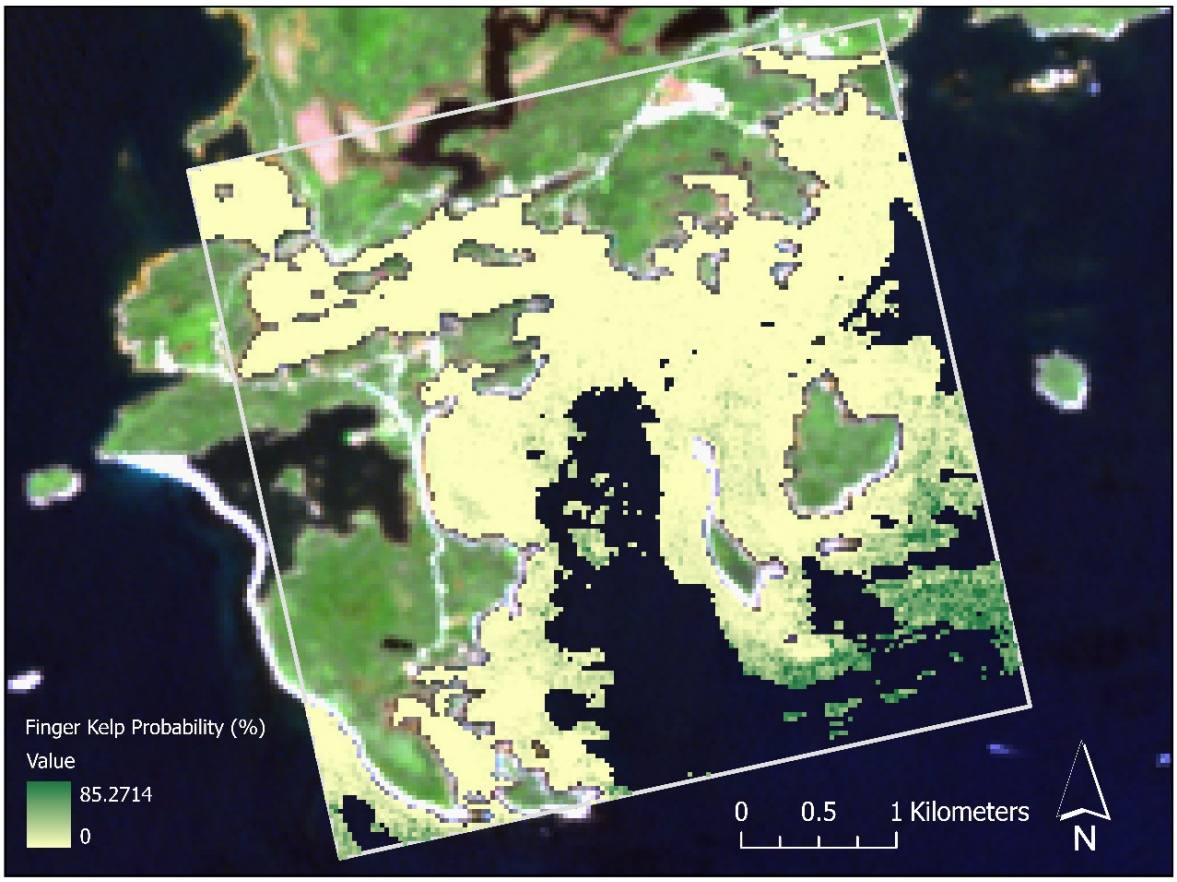


Figure 17. Output predicted probability map for finger kelp (model M), which had recall of >70% during the testing stage.

Finger kelp was incorrectly classified as eelgrass by some models during the final output classification; for example, the model M prediction at points K6-6 and K6-7 (see Figure 18). In this area, only finger kelp or 'other vegetation' were observed, with no eelgrass present. Moreover, during the training and testing phase, model M only misclassified finger kelp as 'other vegetation,' not eelgrass. This shows that while there is high recall of both finger kelp and eelgrass (up to 71% and up to 57%), the models still do not always differentiate eelgrass well from finger kelp and sugar kelp, or from 'other vegetation.'

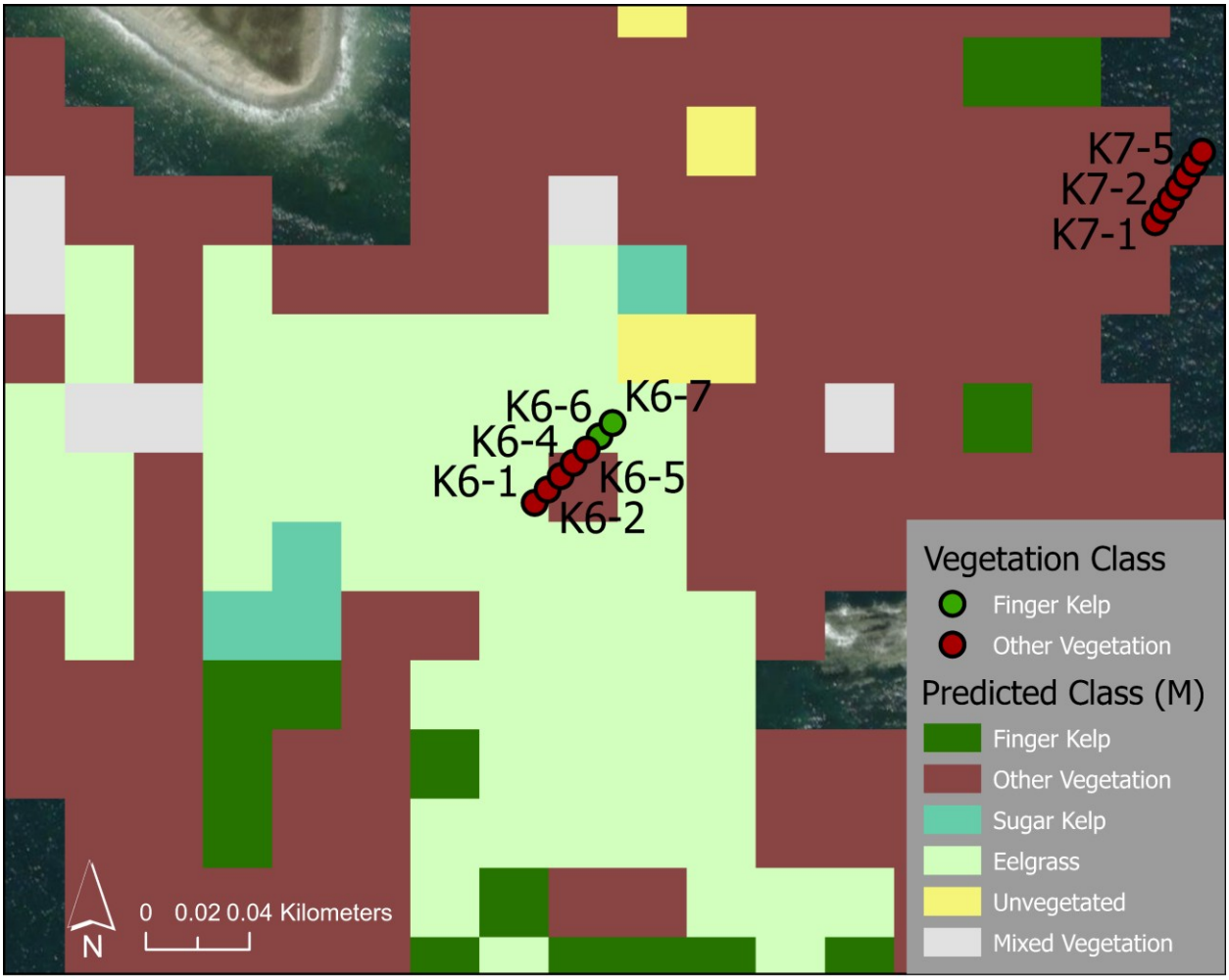


Figure 18. Model M prediction at points K6-1 to K6-7 with reference to original in-situ data.

2.4.4 Landsat-9 model performance

The Landsat-9 models' balanced accuracy was >10% lower than the four best-performing PRISMA models. It showed the lowest recall (<50%) for both finger kelp and eelgrass, the two classes that were detected most successfully by the PRISMA models (see Figure 19), and a very low recall of sugar kelp (<5%). The L9 model was also unable to detect mixed vegetation.

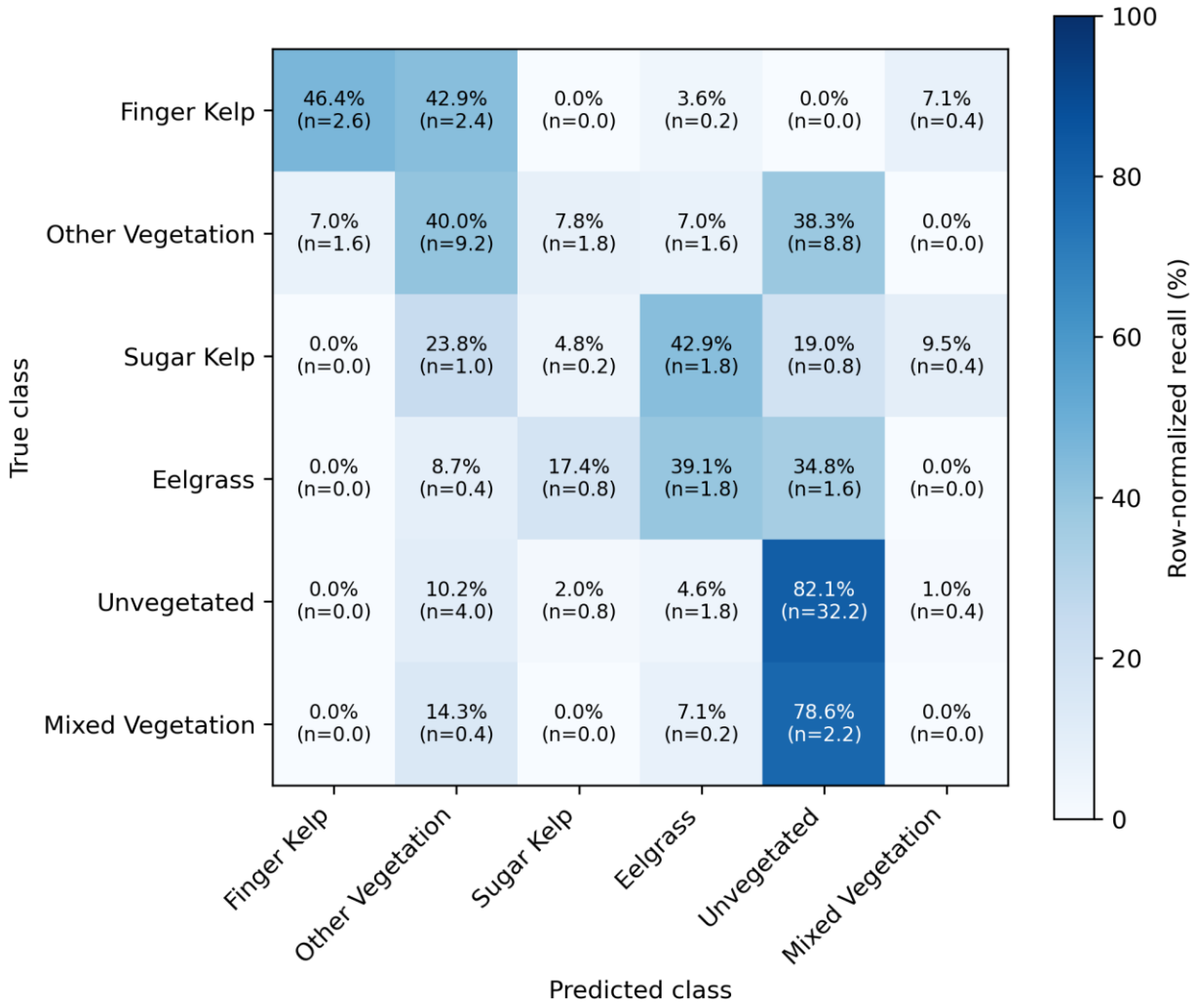


Figure 19. Confusion matrix for the Landsat-9 model, L9. Row-normalized as the values were averaged across all 5-folds of the training and testing stage.

The output map from L9 shows more predicted sugar kelp areas than the PRISMA models; however, given the low recall of sugar kelp during testing, this does not suggest better ability to map sugar kelp, rather it is likely an indication of different noise in the model (see Figure 20). The L9 model detected some areas with success, including the finger kelp patch at the south-east; however, the areas predicted as eelgrass contain more misclassified cells than the PRISMA models' output. There was also more noise and inconsistency between predicted unvegetated and 'other vegetation' at the north-west and north-east corners. The L9 model does not predict a band of 'other vegetation' around shoreline as consistently as the PRISMA models. Overall, there are no consistent benefits, even for a specific class, from using the Landsat-9 models instead of the PRISMA models.

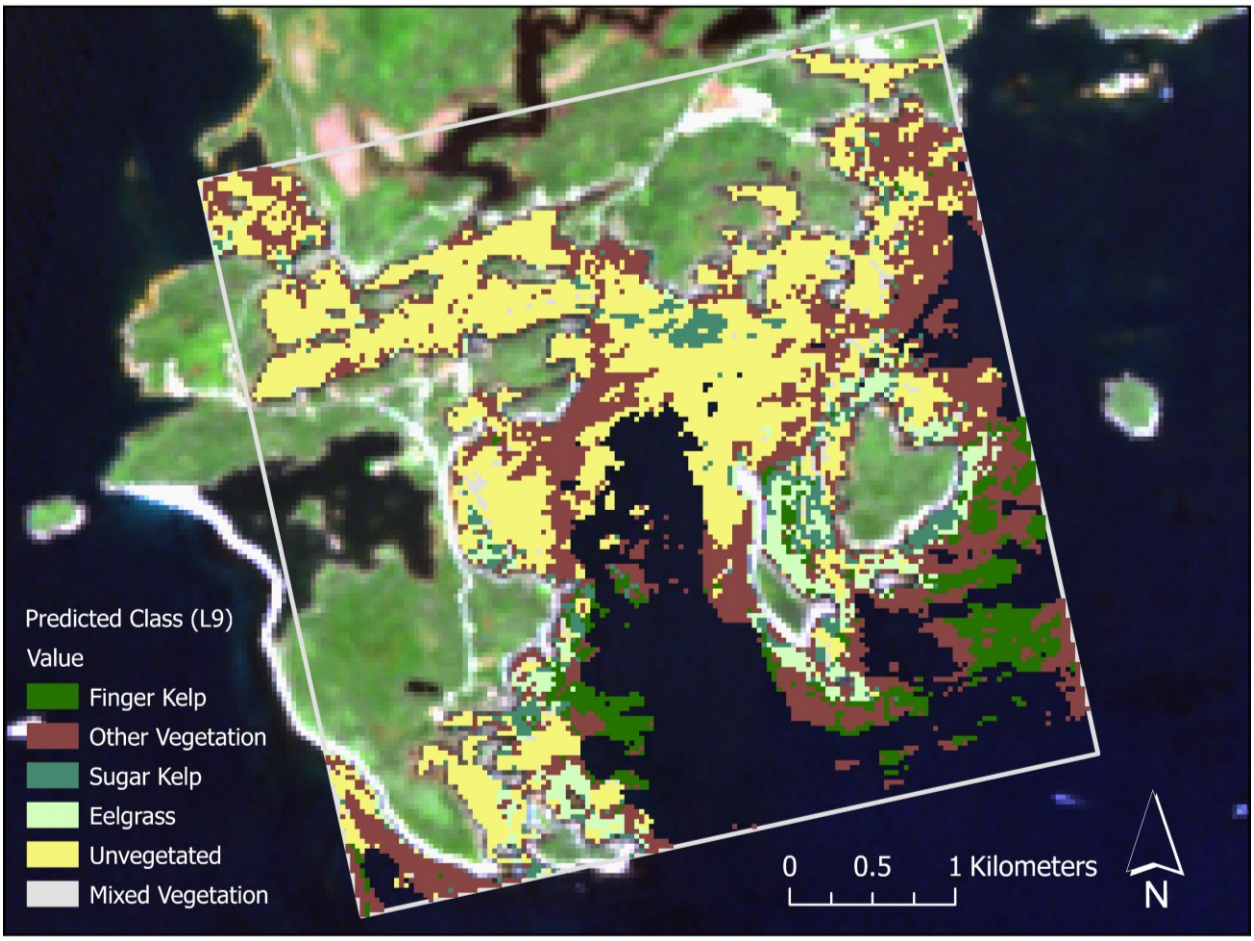


Figure 20. Output classification map from highest performing Landsat-9 model, LD.

2.5 Discussion

2.5.1 In-situ data collection and species distribution

We used a drop camera survey to identify the distribution of our target species within the study area. However, due to time, budget, and weather constraints, the amount of field data collected was limited. Recent pre-existing field datasets collected by other researchers describing kelp species locations were limited to a maximum of one site in the study area (Krumhansl et al., 2024), making it impossible to plan the in-depth survey locations based on confirmed presence of the target species. There was a good dataset for predicted eelgrass area, but not confirmed extent (Gomez et al., 2020). As such, while we managed to collect several observations of each of the target species without much prior knowledge, the total number of observations was small. This impacts the accuracy of the models trained on this data, and due to the localization of field sampling, the models would likely only be applicable to nearby areas along the Eastern Shore of

Nova Scotia, where finger kelp is the dominant type of brown algae and eelgrass is the only species of seagrass.

The equipment used for the drop camera survey was acquired with a low budget; therefore, we used a non-motorized vessel (a sea kayak), and a custom-built drop camera frame with a Go-Pro camera. Due to kayak drift during sampling, some errors were introduced. However, there were some distinct advantages to using this type of setup, namely that it does not require a large budget to undertake the surveys, that the sea-kayak can access much shallower areas compared to a motorized boat, and that the method was effective for capturing high-quality still shots of the bottom in areas up to 15m deep. This method was successful and could be easily employed in other environments, such as small lakes where motorized boats are not permitted, or in shallow environments sensitive to disturbance, including eelgrass beds.

The heterogeneity of habitats in this area also likely affected the accuracy and led to difficulties in differentiating individual species, particularly sugar kelp. Heterogeneity occurred at such small scales, often captured in the same image frame, especially with the habitats of sugar and finger kelp, that even a much higher spatial resolution sensor would observe mixed pixels and be insufficient to separate or distinguish individual species.

2.5.2 Model results and hyperspectral satellite imagery

While the overall accuracy of the models was reasonable (up to 49.2%) for a challenging multi-species classification, the recall of sugar kelp was very low, <10%; as a result, none of the models are useful for mapping sugar kelp. However, the recall of both finger kelp and eelgrass was reasonably high, >57% for the best performing PRISMA models, suggesting that while the ability to differentiate eelgrass from brown algae is moderate, the models were still quite successful at differentiating eelgrass from finger kelp. This is an improvement over results reported by previous studies using multispectral imagery, where eelgrass could not be differentiated from brown algae (Wicaksono et al., 2019; Wilson et al., 2020). Being able to distinguish eelgrass from brown algae alone or identifying the general distribution of the dominant species of brown algae could help significantly towards improving and maintaining knowledge of the whereabouts of marine plants and improving blue carbon contribution estimates.

The feature elimination showed that both single-band and spectral slope features are useful, with many of the most frequently selected features being in the visible range, as expected. These features could be applied directly for future applications in nearby areas where performing feature elimination or reduction is impractical or too computationally intensive. However, ideally a feature reduction or elimination process should be performed each time to ensure the optimal feature set for each application context, and this may vary, especially in different geographical locations with different marine macrophyte species. The improvement in accuracy from using the PRISMA image, compared to the Landsat image, suggests that these narrow and specific spectral features are useful in differentiating between species.

Limitations exist when it comes to the current availability of hyperspectral satellite imagery, as the process to obtain images involves requesting images weeks or months beforehand and is constrained by good weather, priority, and a finite number of allowed observation requests. Therefore, for future studies, it would be necessary to continue tasking hyperspectral satellite images, rather than being able to simply download from a large set of easily available images, which can be done from many multispectral satellites. However, given the improvement of over 10% from using a hyperspectral satellite image over a multispectral satellite image, it may be worth the required pre-planning.

2.5.3 Recommendations for future work

Further studies are needed to determine effective methods to map sugar kelp and to further investigate whether sugar kelp can be distinguished from finger kelp, eelgrass, or other brown algae using hyperspectral satellite imagery. The first recommended step would be to gather a much larger in-situ dataset, as the current dataset is insufficiently large to draw strong conclusions about the models' ability to map all species. Given that a 10% improvement in accuracy was found by using a hyperspectral satellite image compared to a multispectral satellite image, it is recommended to continue testing hyperspectral satellite imagery in further studies. Further studies may find that multi-sensor fusion could be useful, such as integrating a higher spatial resolution multispectral satellite or airborne sensor with a hyperspectral satellite sensor, to more effectively map heterogenous habitat. Future studies should also consider further investigating the effects of heterogeneity on classification accuracy and comparing the results at different spatial scales.

2.6 Conclusion

This study investigated the ability of PRISMA hyperspectral satellite imagery to differentiate important blue carbon marine macrophyte species found near Sheet Harbour, Nova Scotia*: Laminaria digitata* (finger kelp), *Saccharina latissima* (sugar kelp), and *Zostera marina* (eelgrass). Over 400 spectral features from a PRISMA image, including spectral slopes and single band values, were processed through a 5-fold Random Forest (RF) Recursive Feature Elimination (RFE). This process was repeated for six different PRISMA model versions, and a set of the most frequently retained features was identified, showing that both spectral slopes and band values are valuable features, particularly in the visible range. Two Landsat-9 models were also trained and tested. A >10% increase in accuracy was achieved by using the PRISMA data compared to the Landsat-9 data (up to 49.2% balanced accuracy compared to 36.0%). The two highest performing PRISMA models (RD and M) both incorporated depth information. This study established an improvement in differentiating brown algae from eelgrass using satellite imagery: recall of eelgrass was up to 57%, and recall of finger kelp was up to 71%. Further studies should attempt to better differentiate sugar kelp (recall <5%), and the impacts of local habitat heterogeneity on model accuracy should be investigated.

2.7 Author Contributions

Neve Foreman was responsible for research, data collection, analysis, methodology, and writing the original draft. Anders Knudby assisted with conceptualization, provided critical advice, and performed writing reviews and editing.

2.8 References

Adam, E. M., Mutanga, O., Rugege, D., & Ismail, R. (2012). Discriminating the papyrus vegetation (Cyperus papyrus L.) and its co-existent species using random forest and hyperspectral data resampled to HYMAP. *International Journal of Remote Sensing*, *33*(2), 552–569. https://doi.org/10.1080/01431161.2010.543182

Adey, W. H., & Hayek, L. A. C. (2011). Elucidating Marine Biogeography with Macrophytes: Quantitative Analysis of the North Atlantic Supports the Thermogeographic Model and Demonstrates a Distinct Subarctic Region in the Northwestern Atlantic. *Https://Doi.Org/10.1656/045.018.M801*, *18*(mo8), 1–128. https://doi.org/10.1656/045.018.M801

Alongi, D. M. (2018). *Kelp Forests*. 53–57. https://doi.org/10.1007/978-3-319-91698-9_5

Aswatha, S. M., Mukhopadhyay, J., & Biswas, P. K. (2018). Semi-supervised Classification of Land Cover in Multi-spectral Images Using Spectral Slopes. *2017 9th International Conference on Advances in Pattern Recognition, ICAPR 2017*, 338–343. https://doi.org/10.1109/ICAPR.2017.8593093

Bartsch, I., Vogt, J., Pehlke, C., & Hanelt, D. (2013). Prevailing sea surface temperatures inhibit summer reproduction of the kelp Laminaria digitata at Helgoland (North Sea). *Journal of Phycology*, *49*(6), 1061–1073. https://doi.org/10.1111/JPY.12125

Bartsch, I., Wiencke, C., Bischof, K., Buchholz, C. M., Buck, B. H., Eggert, A., Feuerpfeil, P., Hanelt, D., Jacobsen, S., Karez, R., Karsten, U., Molis, M., Roleda, M. Y., Schubert, H., Schumann, R., Valentin, K., Weinberger, F., & Wiese, J. (2008). The genus Laminaria sensu lato: recent insights and developments. *European Journal of Phycology*, *43*(1), 1–86. https://doi.org/10.1080/09670260701711376

Belgiu, M., & Drăgu, L. (2016). Random forest in remote sensing: A review of applications and future directions. *ISPRS Journal of Photogrammetry and Remote Sensing*, *114*, 24–31. https://doi.org/10.1016/J.ISPRSJPRS.2016.01.011

Benediktsson, J. Atli., & Ghamisi, Pedram. (2015). *Spectral-Spatial Classification of Hyperspectral Remote Sensing Images*. Artech House.

Bolton, J. J., & Lüning, K. (1982). Optimal growth and maximal survival temperatures of Atlantic Laminaria species (Phaeophyta) in culture. *Marine Biology*, *66*(1), 89–94. https://doi.org/10.1007/BF00397259/METRICS

Breiman, L. (2001). Random forests. *Machine Learning*, *45*(1), 5–32. https://doi.org/10.1023/A:1010933404324/METRICS

Brickman, D., Wang, Z., & DeTracey, B. (2016). Variability of Current Streams in Atlantic Canadian Waters: A Model Study. *Atmosphere-Ocean*, *54*(3), 218–229. https://doi.org/10.1080/07055900.2015.1094026

Byrnes, J. E., Reed, D. C., Cardinale, B. J., Cavanaugh, K. C., Holbrook, S. J., & Schmitt, R. J. (2011). Climate-driven increases in storm frequency simplify kelp forest food webs. *Global Change Biology*, *17*(8), 2513–2524. https://doi.org/10.1111/J.1365-2486.2011.02409.X

Canadian Hydrographic Service. (2025a). Non-Navigational (NONNA) 10m Bathymetric Data. In *Open Government Portal*. Fisheries and Oceans Canada. https://open.canada.ca/data/en/dataset/d3881c4c-650d-4070-bf9b-1e00aabf0a1d

Canadian Hydrographic Service. (2025b). *Sheet Harbour (00510)*. Government of Canada Tidal Stations. https://www.tides.gc.ca/en/stations/00510

Chao Rodríguez, Y., Domínguez Gómez, J. A., Sánchez-Carnero, N., & Rodríguez-Pérez, D. (2017). A comparison of spectral macroalgae taxa separability methods using an

extensive spectral library. *Algal Research*, *26*, 463–473. https://doi.org/10.1016/J.ALGAL.2017.04.021

Chen, Z., Kwon, Y. O., Chen, K., Fratantoni, P., Gawarkiewicz, G., & Joyce, T. M. (2020). Long-Term SST Variability on the Northwest Atlantic Continental Shelf and Slope. *Geophysical Research Letters*, *47*(1), e2019GL085455. https://doi.org/10.1029/2019GL085455

Choate, M. J., Rengarajan, R., Storey, J. C., & Lubke, M. (2023). Landsat 9 Geometric Commissioning Calibration Updates and System Performance Assessment. *Remote Sensing 2023, Vol. 15, Page 3524*, *15*(14), 3524. https://doi.org/10.3390/RS15143524

Clarke, K., Hennessy, A., McGrath, A., Daly, R., Gaylard, S., Turner, A., Cameron, J., Lewis, M., & Fernandes, M. B. (2021). Using hyperspectral imagery to investigate large-scale seagrass cover and genus distribution in a temperate coast. *Scientific Reports 2021 11:1*, *11*(1), 1–9. https://doi.org/10.1038/s41598-021-83728-6

Department of Fisheries and Oceans Canada. (2009). Does eelgrass (Zostera marina) meet the criteria as an ecologically significant species? *Centre for Science Advice Gulf Region*, *Report 2009/018*.

Department of Fisheries and Oceans Canada. (2024). *Establishing new Marine Protected Areas*. https://www.dfo-mpo.gc.ca/oceans/aoi-si/index-eng.html

Diehl, N., Li, H., Scheschonk, L., Burgunter-Delamare, B., Niedzwiedz, S., Forbord, S., Sæther, M., Bischof, K., & Monteiro, C. (2024). The sugar kelp Saccharina latissima I: recent advances in a changing climate. *Annals of Botany*, *133*(1), 183–212. https://doi.org/10.1093/AOB/MCAD173

Dierssen, H. M., Ackleson, S. G., Joyce, K. E., Hestir, E. L., Castagna, A., Lavender, S., & McManus, M. A. (2021). Living up to the Hype of Hyperspectral Aquatic Remote Sensing: Science, Resources and Outlook. *Frontiers in Environmental Science*, *9*, 649528. https://doi.org/10.3389/FENVS.2021.649528/BIBTEX

Drew, E. A. (1983). Physiology of Laminaria. *Marine Ecology*, *4*(3), 227–250. https://doi.org/10.1111/J.1439-0485.1983.TB00298.X

Duarte, C. M. (2017). Reviews and syntheses: Hidden forests, the role of vegetated coastal habitats in the ocean carbon budget. *Biogeosciences*, *14*(2), 301–301.

Duarte, C. M., & Krause-Jensen, D. (2017). Export from seagrass meadows contributes to marine carbon sequestration. *Frontiers in Marine Science*, *4*(JAN), 217090. https://doi.org/10.3389/FMARS.2017.00013/BIBTEX

Environment and Climate Change Canada. (2008). *Atlantic Shoreline Classification*. Open Government Portal. https://open.canada.ca/data/en/dataset/30449352-2556-42df-9ffe-47ea8e696f91

Filbee-Dexter, K., & Wernberg, T. (2018). Rise of Turfs: A New Battlefront for Globally Declining Kelp Forests. *BioScience*, *68*(2), 64–76. https://doi.org/10.1093/BIOSCI/BIX147

Filbee-Dexter, K., Wernberg, T., Grace, S. P., Thormar, J., Fredriksen, S., Narvaez, C. N., Feehan, C. J., & Norderhaug, K. M. (2020). Marine heatwaves and the collapse of marginal North Atlantic kelp forests. *Scientific Reports 2020 10:1*, *10*(1), 1–11. https://doi.org/10.1038/s41598-020-70273-x

Fyfe, S. K. (2003). Spatial and temporal variation in spectral reflectance: Are seagrass species spectrally distinct? *Limnology and Oceanography*, *48*(1), 464–479. https://doi.org/10.4319/LO.2003.48.1_PART_2.0464

Giardino, C., Brando, V. E., Gege, P., Pinnel, N., Hochberg, E., Knaeps, E., Reusen, I., Doerffer, R., Bresciani, M., Braga, F., Foerster, S., Champollion, N., & Dekker, A. (2019). Imaging Spectrometry of Inland and Coastal Waters: State of the Art, Achievements and Perspectives. *Surveys in Geophysics*, *40*(3), 401–429. https://doi.org/10.1007/S10712-018-9476-0/TABLES/1

Giardino, C., Candiani, G., Bresciani, M., Lee, Z., Gagliano, S., & Pepe, M. (2012). BOMBER: A tool for estimating water quality and bottom properties from remote sensing images. *Computers & Geosciences*, *45*, 313–318. https://doi.org/10.1016/J.CAGEO.2011.11.022

Gomez, C., Guijarro-Sabaniel, J., & Wong, M. (2020). National Eelgrass Task (NET) Force: engagement in support of a dynamic map of eelgrass distribution in Canada to support monitoring, research and decision making. *Canadian Technical Report of Fisheries and Aquatic Sciences*, (3437).

Granitto, P. M., Furlanello, C., Biasioli, F., & Gasperi, F. (2006). Recursive feature elimination with random forest for PTR-MS analysis of agroindustrial products. *Chemometrics and Intelligent Laboratory Systems*, *83*(2), 83–90. https://doi.org/10.1016/J.CHEMOLAB.2006.01.007

Hammer, K. J., Borum, J., Hasler-Sheetal, H., Shields, E. C., Sand-Jensen, K., & Moore, K. A. (2018). High temperatures cause reduced growth, plant death and metabolic changes in eelgrass Zostera marina. *Marine Ecology Progress Series*, *604*, 121–132. https://doi.org/10.3354/MEPS12740

Han, G., Loder, J. W., & Smith, P. C. (1999). Seasonal-Mean Hydrography and Circulation in the Gulf of St. Lawrence and on the Eastern Scotian and Southern Newfoundland Shelves. *Journal of Physical Oceanography*, *29*(6), 1279–1301. https://doi.org/10.1175/1520-0485(1999)029

He, X., Karthick, M., & Shanmugam, P. (2024). Enhanced POLYMER atmospheric correction algorithm for water-leaving radiance retrievals from hyperspectral/multispectral remote sensing data in inland and coastal waters. *Optics*

Express, Vol. 32, Issue 5, Pp. 7659-7681, *32*(5), 7659–7681. https://doi.org/10.1364/OE.504088

Hogrefe, K. R., Ward, D. H., Donnelly, T. F., & Dau, N. (2014). Establishing a Baseline for Regional Scale Monitoring of Eelgrass (Zostera marina) Habitat on the Lower Alaska Peninsula. *Remote Sensing 2014, Vol. 6, Pages 12447-12477*, *6*(12), 12447–12477. https://doi.org/10.3390/RS61212447

Hughes, G. F. (1968). On the Mean Accuracy of Statistical Pattern Recognizers. *IEEE Transactions on Information Theory*, *14*(1), 55–63. https://doi.org/10.1109/TIT.1968.1054102

Jabbari, A., Wu, Y., Wong, M. C., & Dowd, M. (2024). Modelling water temperature dynamics for eelgrass (Zostera marina) areas in the nearshore Scotian Shelf. *Frontiers in Marine Science*, *11*, 1374884. https://doi.org/10.3389/FMARS.2024.1374884/BIBTEX

James, N. C., & Whitfield, A. K. (2023). The role of macroalgae as nursery areas for fish species within coastal seascapes. *Cambridge Prisms: Coastal Futures*, *1*, e3. https://doi.org/10.1017/CFT.2022.3

Jay, S., Guillaume, M., Minghelli, A., Deville, Y., Chami, M., Lafrance, B., & Serfaty, V. (2017). Hyperspectral remote sensing of shallow waters: Considering environmental noise and bottom intra-class variability for modeling and inversion of water reflectance. *Remote Sensing of Environment*, *200*, 352–367. https://doi.org/10.1016/J.RSE.2017.08.020

Jeffery, N. W., Heaslip, S. G., Stevens, L. A., & Stanley, R. R. E. (2020). *Biophysical and Ecological Overview of the Eastern Shore Islands Area of Interest (AOI)*. https://waves-vagues.dfo-mpo.gc.ca/library-bibliotheque/40885045.pdf

Keogh, E., & Mueen, A. (2017). Curse of Dimensionality. *Encyclopedia of Machine Learning and Data Mining*, 314–315. https://doi.org/10.1007/978-1-4899-7687-1_192/FIGURES/322

Kim, M., Park, S., Anderson, C., & Stensaas, G. L. (2022). System characterization report on PRecursore IperSpettrale della Missione Applicativa (PRISMA). *Open-File Report*, *2022*. https://doi.org/10.3133/OFR20211030K

King, N. G., Teagle, H., Hawkins, S. J., & Smale, D. A. (2025). Foundation species loss alters algal community structure and dynamics at a trailing range edge. *Journal of Ecology*, *113*(12), 3858–3872. https://doi.org/10.1111/1365-2745.70199

Kirk, J. T. O. (1983). *Light and Photosynthesis in Aquatic Ecosystems* (1st ed.). Cambridge University Press. https://doi.org/10.1017/CBO9780511623370

Krause-Jensen, D., & Duarte, C. M. (2016). Substantial role of macroalgae in marine carbon sequestration. *Nature Geoscience 2016 9:10*, *9*(10), 737–742. https://doi.org/10.1038/ngeo2790

Krumhansl, K. A., Brooks, C. M., Lowen, J. B., O'Brien, J. M., Wong, M. C., & DiBacco, C. (2024). Loss, resilience and recovery of kelp forests in a region of rapid ocean warming. *Annals of Botany*, *133*(1), 73–92. https://doi.org/10.1093/AOB/MCAD170

Krumhansl, K. A., Dowd, M., & Wong, M. C. (2020). A characterization of the physical environment at eelgrass (Zostera marina) sites along the Atlantic coast of Nova Scotia Maritimes Region. *Fisheries and Oceans Canada Canadian Technical Report of Fisheries and Aquatic Sciences, 3361*.

Krumhansl, K. A., Wong, M. C., M Picard, M. M., Fraser, M., Gabriel, C.-E., Wu, Y., & Azetsu-Scott, K. (2026). Blue carbon sequestration dominated by dissolved organic carbon pathways for kelp forests and eelgrass meadows in Nova Scotia, Canada. *Communications Earth & Environment 2026 7:1*, *7*(1), 98-. https://doi.org/10.1038/s43247-025-03122-2

Lewis, P. H., Roberts, B. P., Moore, P. J., Pike, S., Scarth, A., Medcalf, K., & Cameron, I. (2023). Combining unmanned aerial vehicles and satellite imagery to quantify areal extent of intertidal brown canopy forming macroalgae. *Remote Sensing in Ecology and Conservation*, *9*(4), 540–1092. https://doi.org/10.1002/RSE2.327

Li, R., Liu, J. K., Sukcharoenpong, A., Yuan, J., Zhu, H., & Zhang, S. (2012). A Systematic Approach toward Detection of Seagrass Patches from Hyperspectral Imagery. *Marine Geodesy*, *35*(3), 271–286. https://doi.org/10.1080/01490419.2012.699019

Loizzo, R., Guarini, R., Longo, F., Scopa, T., Formaro, R., Facchinetti, C., & Varacalli, G. (2018). Prisma: The Italian hyperspectral mission. *IGARSS 2018 - 2018 IEEE International Geoscience and Remote Sensing Symposium*, 175–178. https://doi.org/10.1109/IGARSS.2018.8518512

Lyzenga, D. R. (1978). Passive remote sensing techniques for mapping water depth and bottom features. *Applied Optics, Vol. 17, Issue 3, Pp. 379-383*, *17*(3), 379–383. https://doi.org/10.1364/AO.17.000379

Maldonado, S., & Weber, R. (2009). A wrapper method for feature selection using Support Vector Machines. *Information Sciences*, *179*(13), 2208–2217. https://doi.org/10.1016/J.INS.2009.02.014

Malyshev, A., & Quijón, P. A. (2011). Disruption of essential habitat by a coastal invader: new evidence of the effects of green crabs on eelgrass beds. *ICES Journal of Marine Science*, *68*(9), 1852–1856. https://doi.org/10.1093/ICESJMS/FSR126

Marcello, J., Eugenio, F., Martín, J., & Marqués, F. (2018). Seabed Mapping in Coastal Shallow Waters Using High Resolution Multispectral and Hyperspectral Imagery.

Remote Sensing 2018, Vol. 10, Page 1208, *10*(8), 1208. https://doi.org/10.3390/RS10081208

Maritorena, S., Morel, A., & Gentili, B. (1994). Diffuse reflectance of oceanic shallow waters: Influence of water depth and bottom albedo. *Limnology and Oceanography*, *39*(7), 1689–1703. https://doi.org/10.4319/LO.1994.39.7.1689

Masek, J. G., Wulder, M. A., Markham, B., McCorkel, J., Crawford, C. J., Storey, J., & Jenstrom, D. T. (2020). Landsat 9: Empowering open science and applications through continuity. *Remote Sensing of Environment*, *248*, 111968. https://doi.org/10.1016/J.RSE.2020.111968

Matheson, K., McKenzie, C. H., Gregory, R. S., Robichaud, D. A., Bradbury, I. R., Snelgrove, P. V. R., & Rose, G. A. (2016). Linking eelgrass decline and impacts on associated fish communities to European green crab Carcinus maenas invasion. *Marine Ecology Progress Series*, *548*, 31–45. https://doi.org/10.3354/MEPS11674

Mathieson, A. C., & Dawes, C. J. (2020). Biology and ecology of Northwest Atlantic seaweeds. *Handbook of Algal Science, Technology and Medicine*, 71–90. https://doi.org/10.1016/B978-0-12-818305-2.00005-X

Murphy, G. E. P., Dunic, J. C., Adamczyk, E. M., Bittick, S. J., Côté, I. M., Cristiani, J., Geissinger, E. A., Gregory, R. S., Lotze, H. K., O'Connor, M. I., Araújo, C. A. S., Rubidge, E. M., Templeman, N. D., & Wong, M. C. (2021). From coast to coast to coast: Ecology and management of seagrass ecosystems across Canada. *Facets*, *6*(1), 139–179. https://doi.org/10.1139/facets-2020-0020

Niu, S., Zhang, P., Liu, J., Guo, D., & Zhang, X. (2012). The effect of temperature on the survival, growth, photosynthesis, and respiration of young seedlings of eelgrass Zostera marina L. *Aquaculture*, *350–353*, 98–108. https://doi.org/10.1016/J.AQUACULTURE.2012.04.010

O'Neill, J. D., & Costa, M. (2013). Mapping eelgrass (Zostera marina) in the Gulf Islands National Park Reserve of Canada using high spatial resolution satellite and airborne imagery. *Remote Sensing of Environment*, *133*, 152–167. https://doi.org/10.1016/J.RSE.2013.02.010

O'Neill, J. D., Costa, M., & Sharma, T. (2011). Remote Sensing of Shallow Coastal Benthic Substrates: In situ Spectra and Mapping of Eelgrass (Zostera marina) in the Gulf Islands National Park Reserve of Canada. *Remote Sensing 2011, Vol. 3, Pages 975-1005*, *3*(5), 975–1005. https://doi.org/10.3390/RS3050975

Pal, M., & Foody, G. M. (2010). Feature selection for classification of hyperspectral data by SVM. *IEEE Transactions on Geoscience and Remote Sensing*, *48*(5), 2297–2307. https://doi.org/10.1109/TGRS.2009.2039484

Pedregosa, F., Michel, V., Grisel, O., Blondel, M., Prettenhofer, P., Weiss, R., Vanderplas, J., Cournapeau, D., Pedregosa, F., Varoquaux, G., Gramfort, A., Thirion, B., Grisel, O.,

Dubourg, V., Passos, A., Brucher, M., Perrot, M., & Duchesnay, É. (2011). Scikit-learn: Machine Learning in Python. *Journal of Machine Learning Research*, *12*(85), 2825–2830. http://jmlr.org/papers/v12/pedregosa11a.html

Peng, J., Li, J., Krause, J. R., Lyons, M. B., Murray, N. J., Schill, S. R., Roelfsema, C. M., & Asner, G. P. (2026). Global high-resolution mapping of seagrass to support conservation. *Nature 2026 655:8123*, *655*(8123), 663–669. https://doi.org/10.1038/S41586-026-10704-3

Peñuelas, J., Gamon, J. A., Griffin, K. L., & Field, C. B. (1993). Assessing community type, plant biomass, pigment composition, and photosynthetic efficiency of aquatic vegetation from spectral reflectance. *Remote Sensing of Environment*, *46*(2), 110–118. https://doi.org/10.1016/0034-4257(93)90088-F

Phinn, S., Roelfsema, C., Dekker, A., Brando, V., & Anstee, J. (2008). Mapping seagrass species, cover and biomass in shallow waters: An assessment of satellite multi-spectral and airborne hyper-spectral imaging systems in Moreton Bay (Australia). *Remote Sensing of Environment*, *112*(8), 3413–3425. https://doi.org/10.1016/J.RSE.2007.09.017

Poona, N. K., Van Niekerk, A., Nadel, R. L., & Ismail, R. (2016). Random Forest (RF) Wrappers for Waveband Selection and Classification of Hyperspectral Data. *Applied Spectroscopy*, *70*(2), 322–333. https://doi.org/10.1177/0003702815620545

Pullanagari, R. R., Kereszturi, G., & Yule, I. (2018). Integrating Airborne Hyperspectral, Topographic, and Soil Data for Estimating Pasture Quality Using Recursive Feature Elimination with Random Forest Regression. *Remote Sensing 2018, Vol. 10, Page 1117*, *10*(7), 1117. https://doi.org/10.3390/RS10071117

Qian, S. E. (2022). Overview of Hyperspectral Imaging Remote Sensing from Satellites. *Advances in Hyperspectral Image Processing Techniques*, 41–66. https://doi.org/10.1002/9781119687788.CH2

Reichstetter, M., C S Fearns, P. R., Weeks, S. J., W McKinna, L. I., Roelfsema, C., Furnas, M., Mishra, D. R., Gould Jr, R. W., Gloaguen, R., & Thenkabail, P. S. (2015). Bottom Reflectance in Ocean Color Satellite Remote Sensing for Coral Reef Environments. *Remote Sensing 2015, Vol. 7, Pages 16756-16777*, *7*(12), 16756–16777. https://doi.org/10.3390/RS71215852

Röhr, M. E., Holmer, M., Baum, J. K., Björk, M., Chin, D., Chalifour, L., Cimon, S., Cusson, M., Dahl, M., Deyanova, D., Duffy, J. E., Eklöf, J. S., Geyer, J. K., Griffin, J. N., Gullström, M., Hereu, C. M., Hori, M., Hovel, K. A., Hughes, A. R., … Boström, C. (2018). Blue Carbon Storage Capacity of Temperate Eelgrass (Zostera marina) Meadows. *Global Biogeochemical Cycles*, *32*(10), 1457–1475. https://doi.org/10.1029/2018GB005941

Rowan, G. S. L., & Kalacska, M. (2021). A Review of Remote Sensing of Submerged Aquatic Vegetation for Non-Specialists. *Remote Sensing 2021, Vol. 13, Page 623*, *13*(4), 623. https://doi.org/10.3390/RS13040623

Sarker, I. H. (2021). Deep Learning: A Comprehensive Overview on Techniques, Taxonomy, Applications and Research Directions. *Sn Computer Science*, *2*(6), 420. https://doi.org/10.1007/S42979-021-00815-1

Schalles, J. F. (2006). Optical Remote Sensing Techniques To Estimate Phytoplankton Chlorophyll A Concentrations in Coastal Waters with Varying Suspended Matter and CDOM Concentrations. In *Remote Sensing and Digital Image Processing* (Vol. 9, pp. 27–79). https://doi.org/10.1007/1-4020-3968-9_3

Schmidt, K. S., & Skidmore, A. K. (2003). Spectral discrimination of vegetation types in a coastal wetland. *Remote Sensing of Environment*, *85*(1), 92–108. https://doi.org/10.1016/S0034-4257(02)00196-7

Short, F. T., Polidoro, B., Livingstone, S. R., Carpenter, K. E., Bandeira, S., Bujang, J. S., Calumpong, H. P., Carruthers, T. J. B., Coles, R. G., Dennison, W. C., Erftemeijer, P. L. A., Fortes, M. D., Freeman, A. S., Jagtap, T. G., Kamal, A. H. M., Kendrick, G. A., Judson Kenworthy, W., La Nafie, Y. A., Nasution, I. M., … Zieman, J. C. (2011). Extinction risk assessment of the world's seagrass species. *Biological Conservation*, *144*(7), 1961–1971. https://doi.org/10.1016/J.BIOCON.2011.04.010

Silva, T. S. F., Costa, M. P. F., Melack, J. M., & Novo, E. M. L. (2008). Remote sensing of aquatic vegetation: theory and applications. *Environ Monit Assess*, *140*, 131–145. https://doi.org/10.1007/s10661-007-9855-3

Spitzer, D., & Dirks, R. W. (1987). Bottom influence on the reflectance of the sea. *International Journal of Remote Sensing*, *8*(3), 279–290. https://doi.org/10.1080/01431168708948642

Storch, T., Honold, H. P., Chabrillat, S., Habermeyer, M., Tucker, P., Brell, M., Ohndorf, A., Wirth, K., Betz, M., Kuchler, M., Mühle, H., Carmona, E., Baur, S., Mücke, M., Löw, S., Schulze, D., Zimmermann, S., Lenzen, C., Wiesner, S., … Fischer, S. (2023). The EnMAP imaging spectroscopy mission towards operations. *Remote Sensing of Environment*, *294*, 113632. https://doi.org/10.1016/J.RSE.2023.113632

Thomas, A. C., Pershing, A. J., Friedland, K. D., Nye, J. A., Mills, K. E., Alexander, M. A., Record, N. R., Weatherbee, R., & Elisabeth Henderson, M. (2017). Seasonal trends and phenology shifts in sea surface temperature on the North American northeastern continental shelf. *Elementa*, *5*. https://doi.org/10.1525/ELEMENTA.240/112445

Timmer, B., Reshitnyk, L. Y., Hessing-Lewis, M., Juanes, F., & Costa, M. (2022). Comparing the Use of Red-Edge and Near-Infrared Wavelength Ranges for Detecting Submerged Kelp Canopy. *Remote Sensing*, *14*(9). https://doi.org/10.3390/rs14092241

Uhl, F., Bartsch, I., & Oppelt, N. (2016). Submerged Kelp Detection with Hyperspectral Data. *Remote Sensing 2016, Vol. 8, Page 487*, *8*(6), 487. https://doi.org/10.3390/RS8060487

Vahtmäe, E., Paavel, B., & Kutser, T. (2020). How much benthic information can be retrieved with hyperspectral sensor from the optically complex coastal waters? *Journal of Applied Remote Sensing*, *14*(01), 1. https://doi.org/10.1117/1.JRS.14.016504

Vanhellemont, Q. (2019). Adaptation of the dark spectrum fitting atmospheric correction for aquatic applications of the Landsat and Sentinel-2 archives. *Remote Sensing of Environment*, *225*, 175–192. https://doi.org/10.1016/J.RSE.2019.03.010

Varunan, T., & Shanmugam, P. (2020). *Modelling the optical properties of coral reefs and its implication for optical remote sensing*. https://doi.org/10.1016/j.ecss.2020.107054

Wernberg, T., Krumhansl, K., Filbee-Dexter, K., & Pedersen, M. F. (2019). Status and Trends for the World's Kelp Forests. *World Seas: An Environmental Evaluation Volume III: Ecological Issues and Environmental Impacts*, 57–78. https://doi.org/10.1016/B978-0-12-805052-1.00003-6

Wicaksono, P., Aryaguna, P. A., & Lazuardi, W. (2019). Benthic Habitat Mapping Model and Cross Validation Using Machine-Learning Classification Algorithms. *Remote Sensing 2019, Vol. 11, Page 1279*, *11*(11), 1279. https://doi.org/10.3390/RS11111279

Williams, D. J., Rybicki, N. B., Lombana, A. V., O'Brien, T. M., & Gomez, R. B. (2003). Preliminary investigation of submerged aquatic vegetation mapping using hyperspectral remote sensing. *Environmental Monitoring and Assessment*, *81*(1–3), 383–392. https://doi.org/10.1023/A:1021318217654/METRICS

Wilson, K. L., & Lotze, H. K. (2019). Climate change projections reveal range shifts of eelgrass Zostera marina in the Northwest Atlantic. *Marine Ecology Progress Series*, *620*, 47–62. https://doi.org/10.3354/MEPS12973

Wilson, K. L., Skinner, M. A., & Lotze, H. K. (2019a). Eelgrass (Zostera marina) and benthic habitat mapping in Atlantic Canada using high-resolution SPOT 6/7 satellite imagery. *Estuarine, Coastal and Shelf Science*, *226*, 106292. https://doi.org/10.1016/J.ECSS.2019.106292

Wilson, K. L., Skinner, M. A., & Lotze, H. K. (2019b). Projected 21st-century distribution of canopy-forming seaweeds in the Northwest Atlantic with climate change. *Diversity and Distributions*, *25*(4), 582–602. https://doi.org/10.1111/DDI.12897

Wilson, K. L., Wong, M. C., & Devred, E. (2020). Branching Algorithm to Identify Bottom Habitat in the Optically Complex Coastal Waters of Atlantic Canada Using Sentinel-2 Satellite Imagery. *Frontiers in Environmental Science*, *8*, 579856. https://doi.org/10.3389/FENVS.2020.579856/BIBTEX

Wilson, K. L., Wong, M. C., & Devred, E. (2022). Comparing Sentinel-2 and WorldView-3 Imagery for Coastal Bottom Habitat Mapping in Atlantic Canada. *Remote Sensing*, *14*(5), 1254. https://doi.org/10.3390/RS14051254/S1

Wong, P. P., Losada, I. J., Gattuso, J.-P., Hinkel, J., Khattabi, A., McInnes, K. L., Saito, Y., Sallenger, A., Nicholls, R. J., Santos, F., Amez, S., Losada, I., Gattuso, J., Hinkel, J., Khattabi, A., McInnes, K., Saito, Y., Sallenger, A., Barros, V., … Levy, A. (2018). *Coastal Systems and Low-Lying Areas*.

Wright, L. S., Pessarrodona, A., & Foggo, A. (2022). Climate-driven shifts in kelp forest composition reduce carbon sequestration potential. *Global Change Biology*, *28*(18), 5514–5531. https://doi.org/10.1111/GCB.16299

Wu, Y., Knudby, A., & Lapen, D. (2023). Topography-adjusted Monte Carlo simulation of the adjacency effect in remote sensing of coastal and inland waters. *Journal of Quantitative Spectroscopy and Radiative Transfer*, *303*, 108589. https://doi.org/10.1016/J.JQSRT.2023.108589

2.9 Appendix



Figure 21. Example of rocky/sandy unvegetated substrate. Point D11-5.



Figure 22. Example of finger and sugar kelp growing heterogeneously. Point J6-5.

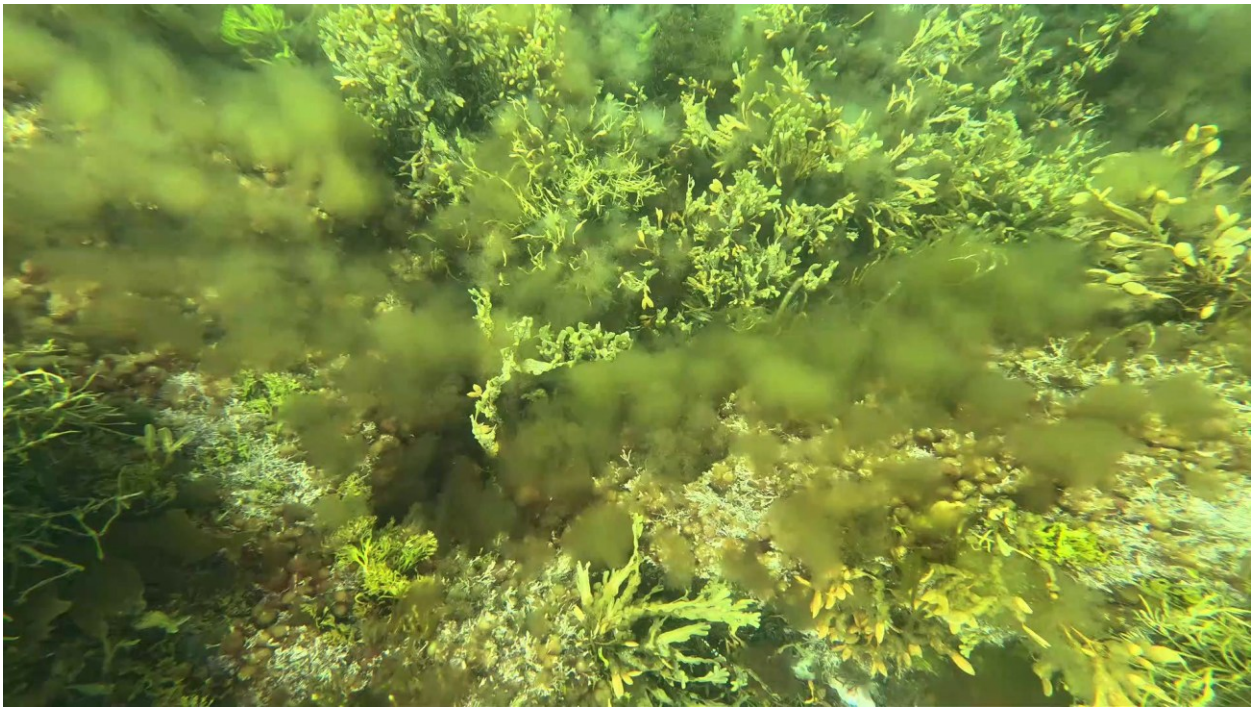


Figure 23. Example of the types of vegetation found at the intertidal zones very close to shore including Fucus distichus (rockweed) and Fucus spiralis (spiral wrack). Point I6-5.

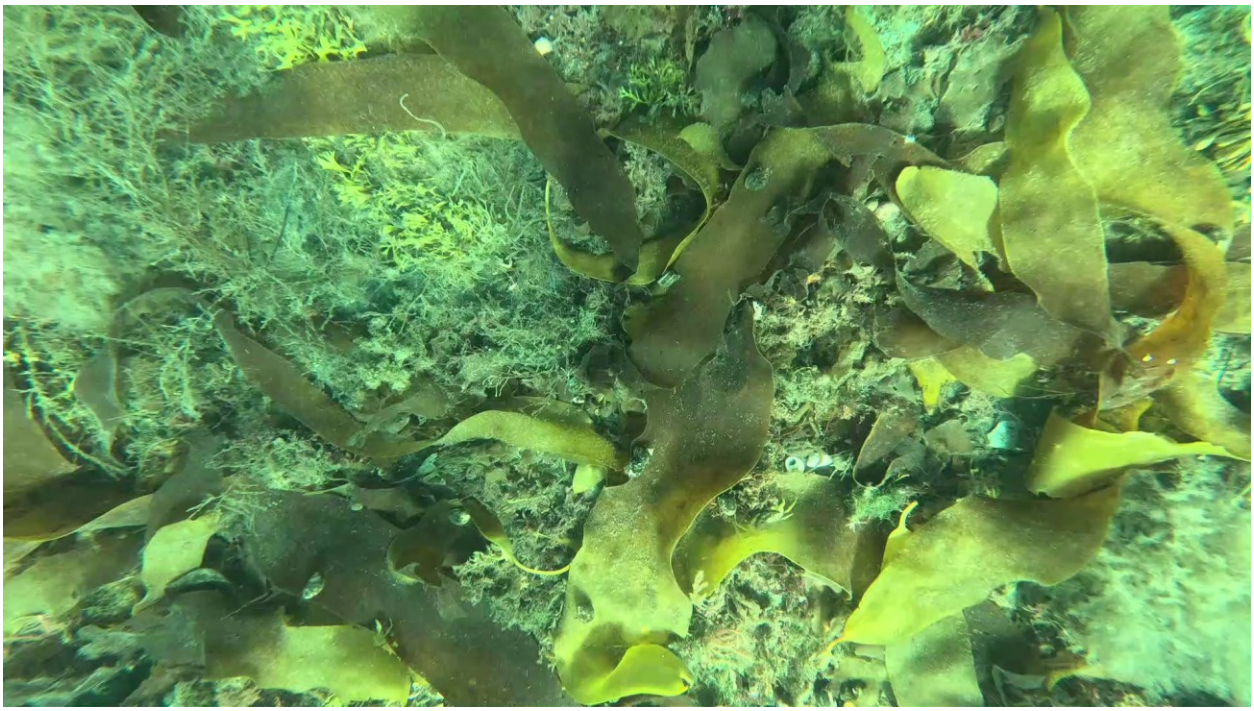


Figure 24. Example of Saccorhiza dermatodea, another brown alga. Point K3-2.



Figure 25. Example of Desmarestia (shown centre). Point M6-6.



Figure 26. Example of Agarum clathratum, another brown alga, shown at right (and upper middle), and other marine macrophyte species, center. Point I3-1.



Figure 27. Invasive Codium Fragile, shown middle. Point K6-4.



Figure 28. Drop camera frame setup attached to kayak.

Chapter 3: Thesis Conclusion

The study of marine macrophytes is becoming increasingly important due to the threat of climate change to intertidal environments and the potential of macrophytes as nature-based climate solutions. *Laminaria digitata* (finger kelp), *Saccharina latissima* (sugar kelp), and *Zostera marina* (eelgrass) are three marine macrophytes whose habitats are known as blue carbon ecosystems due to their outstanding carbon sequestration. These species are found throughout the Eastern Shore Islands (ESI), Nova Scotia, an Area of Interest (AOI) for ecological and biological importance. It is important to distinguish these species, as they have different suitable water temperature ranges and add value to the blue carbon ecosystem for different reasons. Seagrass environments account for up to 33% of total oceanic CO_2 uptake (Röhr et al., 2018); additionally, kelp forests in Nova Scotia are estimated to sequester more carbon than eelgrass by ~1.3 orders of magnitude, largely due to the role of export of dissolved organic

carbon and their large habitat area (Alongi, 2018; Krumhansl et al., 2026; Wright et al., 2022). Unfortunately, due largely to ocean warming and marine heat waves, finger and sugar kelp have had significant habitat loss (Filbee-Dexter & Wernberg, 2018); eelgrass has experienced habitat loss in some areas but is projected to have habitat gain in other areas (Wilson & Lotze, 2019). As eelgrass, sugar kelp, and finger kelp are all foundational species, the loss of populations causes negative changes at the ecosystem level (King et al., 2025; Wernberg et al., 2019). As such, monitoring their populations could also serve as a warning for situations where the whole ecosystem may be at threat.

Due to the threats on finger kelp, sugar kelp, and eelgrass in Eastern Nova Scotia and their differing habitat areas and biological properties, it is important to identify effective methods to monitor these species. While monitoring species does not actively prevent the loss of populations, it allows reliable data about population changes to be recorded and presented as a justification to policy makers in situations such as the creation or expansion of current marine AOIs or protected areas, including the ESI. Previous regional studies using multispectral satellite sensors were unsuccessful at differentiating eelgrass from brown algae (Wicaksono et al., 2019; Wilson et al., 2020), but a hyperspectral satellite sensor offers the spectral resolution (<15nm bandwidths) that is needed to detect subtle differences between species. Additionally, using satellite imagery can be more time and cost effective. While remote sensing based studies of marine macrophytes still need field data to confirm species presence and distribution, developing more effective methods to distinguish between species, particularly kelps, would significantly reduce the number of field surveys required.

Chapter 2 determined that a PRISMA hyperspectral satellite image is useful for mapping the three target species near Sheet Harbour, Nova Scotia, and over a 10% increase in accuracy was found using a hyperspectral image over a Landsat-9 multispectral image. The highest achieved accuracy of 49% is reasonable given the challenging task of differentiating spectrally similar submerged vegetation types, and the current models could be used with some caution to estimate the distribution of eelgrass or finger kelp within the ESI. Moreover, several commonly retained features from the PRISMA image were identified, thus in situations with limited time or computational resources to perform RFE, the most retained features could be used to train future models. However, the exact utility (e.g. whether a given SWIR slope detects emerged vegetation)

of each feature cannot be determined from this type of study alone; it would be necessary to use in-situ reflectance spectra, or isolate certain ‘other vegetation’ species such as rockweed, to determine the specific use of each feature. Future studies should explore these possibilities, as well as multi-sensor fusion and other methods that can help improve the utility of hyperspectral satellite imagery.

There was great difficulty in mapping sugar kelp, demonstrating that challenges still exist when it comes to developing reliable methods for mapping marine macrophytes species in Eastern Nova Scotia. The heterogeneity of habitats in the region is likely one of the greatest reasons it was difficult to identify sugar kelp, and it may not be possible to perform a highly accurate species level differentiation of brown algae without using a higher spatial resolution sensor. It is also possible that the depth at which sugar kelp often grows is a limiting factor, as it is difficult to map species at greater depths. For future studies, the first step would be to gather a much larger in-situ dataset, as the current dataset is insufficient in size to draw strong conclusions about the models’ ability to map all species, especially outside of the general ESI region. In terms of field data annotation, developing an AI based object detection method could be a time saver, using the previously annotated data as training data. After seeing how much of an improvement can be found solely by adding more field data observations, the next steps would be to investigate slightly different methodologies, such as multi-sensor fusion, e.g. integrating a higher spatial resolution multispectral satellite (e.g. Sentinel 2) or airborne sensor with a hyperspectral satellite sensor to more effectively map heterogenous habitat. It would also be useful to test in-situ reflectance spectra of each species locally or narrow down which features are useful for detecting which types of vegetation using a spectrometer or similar device.

AI Use Declaration

Generative AI (i.e. Claude, ChatGPT, Microsoft Copilot) was used during the completion of this thesis in accordance with the Declaration of AI use under the “Artificial Intelligence (AI) Policy for Graduate Students” submitted to and approved by the thesis supervisor and committee members. AI was used mainly to assist with Python coding development, debugging, and very minimally, for writing oversight and searching for literature.